8.

**Analysis of Extreme Wave Climates in Rhode Island
Waters South of Block Island**

By

Annette R. Grilli, Taylor G. Asher, Stephan T. Grilli and Malcolm L. Spaulding

Ocean Engineering
University of Rhode Island

Prepared for

Ocean Special Area Management Plan (SAMP)

October 16, 2010

Executive Summary

This project is one component of comprehensive multidisciplinary studies performed at the University of Rhode Island from 2008 to 2010, to develop a Special Area Management Plan (SAMP) for siting offshore wind farms in Rhode Island waters.

A characterization of extreme wave climates is required when considering such ocean structures, e.g., for designing wind turbine support structures and foundations, or for verifying the long-term stability of their foundations against scour.

A statistical analysis of extreme wave climates off of the southern coast of Block Island was performed, based on wave hindcast data obtained from the US Army Corp of Engineers, Wave Information Studies (WIS) data base. This provided significant wave heights H_s and peak spectral periods T_p for sea states corresponding to long return period events (i.e., 20, 50, 75 and 100 years), arising from a variety of directions. Wave propagation simulations were performed using STWAVE (a steady-state spectral wave model). Various model grids were used, which represented rectangular areas covering from 616 to 978 km^2, surrounding Block Island and the areas where potential wind farms might be sited, to the southwest, south, and southeast of the island.

Simulation results predicted the occurrence, south and southeast of the island, of significant wave heights of at least 8 m for all return periods (upper 95% confidence limit), with significant wave heights exceeding 10 m in the 100 year case. Southwest and west of Block Island, significant wave heights were significantly reduced in all cases, by about 2 meters, due to intense breaking and dissipation over the shallower waters (15 m deep) between Block Island and Montauk Point (eastern end of Long Island) associated with large boulders and quaternary glacial deposits.

Finally, note, WIS provided 20 years (1980-1999) worth of hourly hindcast data for wind speed and direction, significant wave height, and peak spectral period. Hence, the present study and results depend upon the relevance of this time series to describe the present day wave climate around Block Island. In particular no effect of climatic change that may have occurred over the past 10 years, and of any future changes that might occur, on extreme wave parameters is included.

Table of Contents

List of Figures

List of Tables

Abstract

This project is one component of comprehensive multidisciplinary studies performed at the University of Rhode Island from 2008 to 2010, to develop a Special Area Management Plan (SAMP) for siting offshore wind farms in Rhode Island waters.

A characterization of extreme wave climates is required when considering such ocean structures, e.g., for designing wind turbine support structures and foundations, or for verifying the long-term stability of their foundations against scour.

A statistical analysis of extreme wave climates off of the southern coast of Block Island was performed, based on wave hindcast data obtained from the US Army Corp of Engineers, Wave Information Studies (WIS) data base. This provided significant wave heights H_s and peak spectral periods T_p for sea states corresponding to long return period events (i.e., 20, 50, 75 and 100 years), arising from a variety of directions. Wave propagation simulations were performed using STWAVE (a steady-state spectral wave model). Various model grids were used, which represented rectangular areas covering from 616 to 978 km^2, surrounding Block Island and the areas where potential wind farms might be sited, to the southwest, south, and southeast of the island.

Simulation results predicted the occurrence, south and southeast of the island, of significant wave heights of at least 8 m for all return periods (upper 95% confidence limit), with significant wave heights exceeding 10 m in the 100 year case. Southwest and west of Block Island, significant wave heights were significantly reduced in all cases, by about 2 meters, due to intense breaking and dissipation over the shallower waters (15 m deep) between Block Island and Montauk Point (eastern end of Long Island) associated with large boulders and quaternary glacial deposits.

Finally, note, WIS provided 20 years (1980-1999) worth of hourly hindcast data for wind speed and direction, significant wave height, and peak spectral period. Hence, the present study and results depend upon the relevance of this time series to describe the present day wave climate around Block Island. In particular no effect of climatic change that may have occurred over the past 10 years, and of any future changes that might occur, on extreme wave parameters is included.

1 Introduction

1.1 Background

The RI WINDS program was established by the State of Rhode Island, in January 2006, to develop wind energy as a cost-effective means for providing 15% of the state's 1,000 MW energy demand. A Phase I Siting study, performed by Applied Technology and Management (ATM) under this program: (i) showed that most significant wind resources in state waters were in offshore waters; and (ii) identified potential wind farm sites in RI and adjacent federal waters.

The University of Rhode Island was subsequently tasked by the State of RI with developing a more comprehensive and multidisciplinary Ocean Special Area Management Plan (SAMP) (2008-2010) aimed at updating the initial RI WINDS siting study and identifying areas suitable for offshore wind energy development.
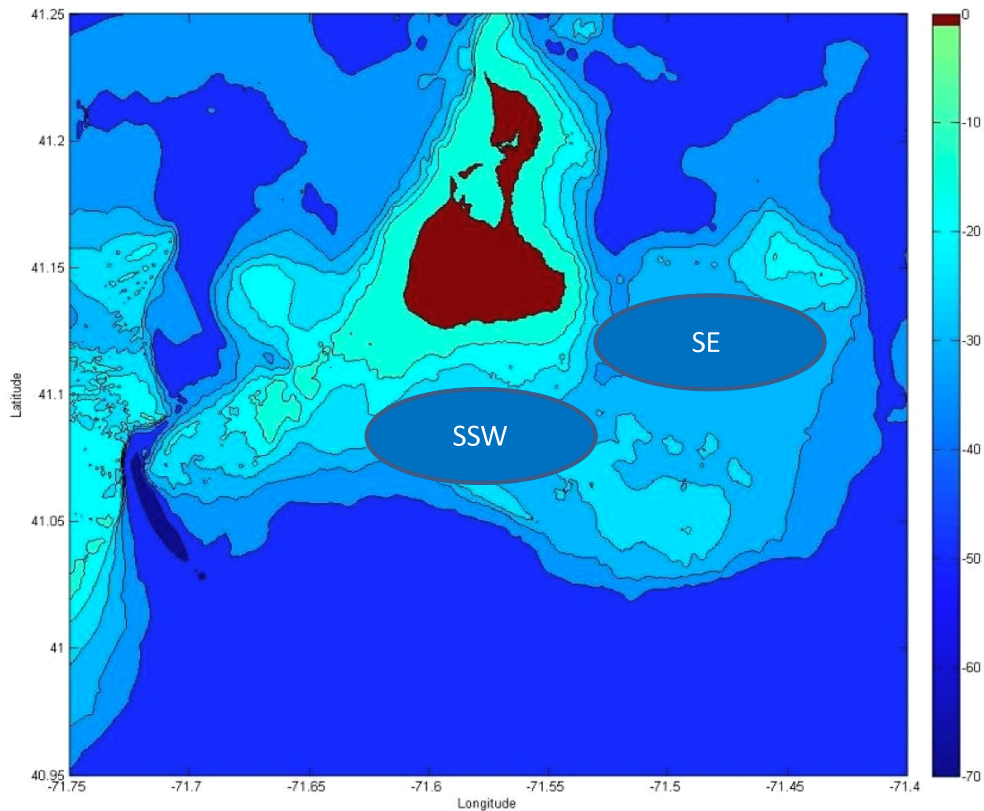
Figure 1.1 : Location of two preliminary sites, SSW and SE of Block Island, under consideration for siting of a wind farm. The map background is the bathymetry of the are, obtained from NOAA's ENC data (depth axis is in meters).

A preliminary evaluation currently in progress as part of the Ocean SAMP, identified two areas in state waters, southeast and south-southwest of Block Island (Fig 1.1), that might be viable as sites for a wind farm. Identification of additional sites in federal waters is also underway. Note, these areas also roughly overlap with the primary and alternate wind farm project sites identified by Deep Water Wind Inc. in their recent proposal to the State of RI.
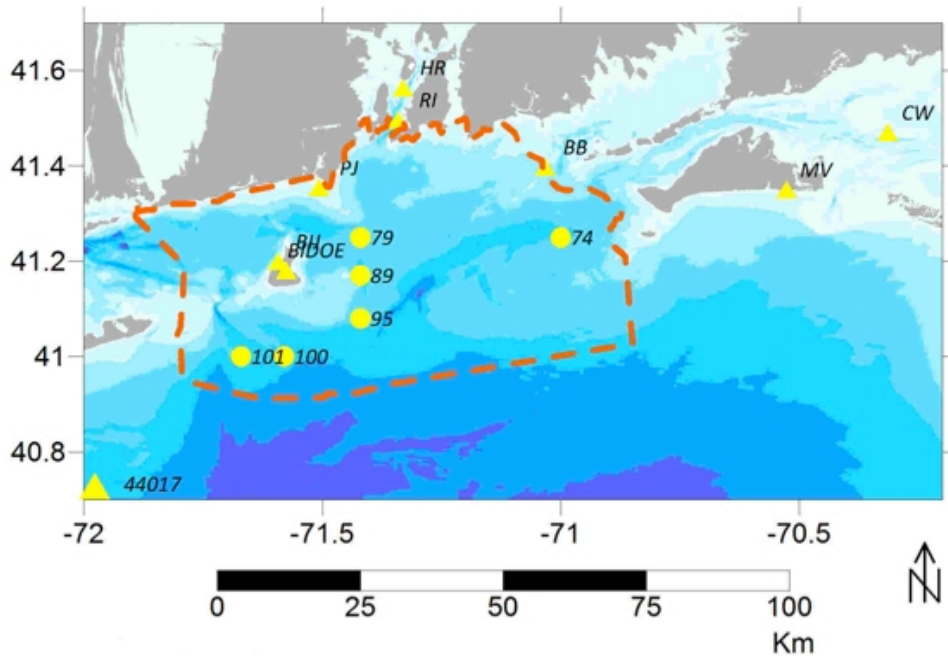
Figure 1.2 : SAMP area (bold dash line) with location of WIS hindcast sites (#74-101; yellow circles) and other SAMP measurement stations (yellow triangles) (Codiga and Ullman, 2010).

Figure 1.2 shows the general SAMP area considered for wind farm siting, in both RI and state waters, with the locations of US Army Corp of Engineers (USACE) Wave Information Study (WIS) hindcast sites (#74-101) and those of other measurement stations for wind waves and current, deployed as part of the SAMP work (e.g., Codiga and Ullman, 2010).

1.2 Study objectives

The main objective of this study is to characterize extreme wave climates near preliminary selected wind farm sites, in RI state waters south of Block Island (Fig. 1.1). This information is essential for designing the foundations and support structures of wind turbines and also useful in screening sites to locate the farm. To do so, we will perform a statistical analysis of extreme wave climates off of the southern coast of Block Island, based on 20 years worth of wave hindcast data obtained from the USACE-WIS data base.

This analysis will provide significant wave heights H_s and peak spectral periods T_p for sea states corresponding to long return period events (i.e., 20, 50, 75 and 100 years), arising from a variety of directions. For each of these cases, we will perform wave detailed propagation simulations over the selected SAMP area (Fig. 1.1) using STWAVE, a steady-state spectral wave model (Appendix A).

It should be pointed out that the present characterization of proposed wind farm sites, based on extreme wave conditions only, is aimed at providing the limiting (i.e., structural survival), or excluding, factors. If an area is not appropriate for extreme conditions, there is no point to further consider it for development. In other SAMP related studies, Grilli et al. (2010) performed hydrodynamic simulations combining wind (RAMS), currents (ROMS), waves (WAVEWATCH III and SWAN), and sediment suspension and transport models, for "normal" conditions corresponding to Fall 2009 and Spring 2010. Results of these simulations were compared to in situ measurements, in particular for waves (see Fig. 1.2 and Ullman and Codiga, 2010), and found to agree well with those. This indicates that the transient spectral numerical wave models routinely used to simulate normal wave conditions in the area (WAVEWATCH III and SWAN), and also to create the WIS data base that serves as a basis for estimating extreme wave climates in the area, are accurate and relevant to the present work.

In view of the bathymetry in the considered areas of Fig. 1.1 and the expected height and period of extreme return period waves (order 10 m and 15 s period), it can be *a priori* inferred that intense breaking will occur both west of the island and in the SSW area identified in Fig. 1.1, and that such sites would be very undesirable for wind farm siting. By contrast, directly south or east of these critical areas, due to the larger water depth, the wave climate should be more appropriate for wind farm siting.

Extreme wave conditions will be analyzed in and around the sites of Fig. 1.1, by performing spectral wave propagation modeling studies. In those, incident wave values will be specified as input (in the form of a directional wave spectra), based on the upper 95 % confidence limit of wave parameters obtained from a statistical analysis of 20 years worth of hindcast wave data available at the nearby USACE-WIS station #101 south of BI (Fig. 1.2).

More specifically, this study has two main parts :

- Estimation of extreme conditions for selected storm return periods (20, 50, 75, and 100 years) in terms of wind and wave climate characteristics, using WIS data at station #101. Key parameters are:
    1. Wind speed and direction
    2. Significant wave height
    3. Peak wave period and direction
    4. Spectral shape
    5. Storm surge

- Prediction of wave climate in an area encompassing the selected sites, by performing simulations with STWAVE (spectral wave propagation program), over a model grid representing the relevant area. Simulations will be performed using the various extreme wave and wind conditions as inputs, and for a series of numerical grids, in order to ensure model convergence.

2 Estimates of Extreme Wave Conditions

2.1 Wind and wave conditions

Estimates of wind and wave parameters were obatined using hindcast data, available south of BI from station #101 (41° latitude North, 71.67° longitude West; Fig. 1.2) of the U.S. Army Corps of Engineers, Wave Information Studies (WIS) [3]. WIS provided 20 years (1980-1999) worth of hourly data for wind speed and direction, significant wave height, and peak spectral period.
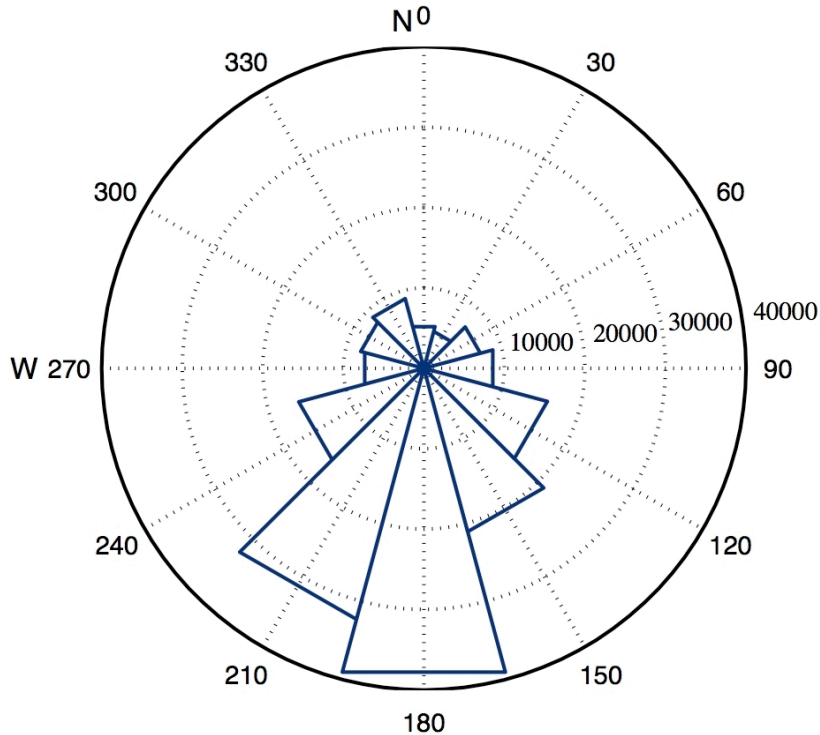
Figure 0.1 : Frequency of wave direction hindcast at WIS station #101, over 1980-1999.

A statistical analysis of waves by direction at WIS station #101 shows the highest frequency of waves arising from the South (Fig. 2.1) (independent from their height). A histogram of significant wave heights at station #101 (Fig. 2.2; all directions included) shows a mean H_s of about 1.2 m over 20 years, while extreme values range up to 8.4 m.

In nature, wind speed and wave height populations closely follow Weibull and Rayleigh probability distributions, respectively (the latter simply being a Weibull distribution with a shape factor equal to 2; see, Rinne (2009), for detail; see, Fig. 2.2, which illustrates the Rayleigh distribution for the wave heights). Individual extreme wind and wave height values, however, are differently distributed. A Gumbel distribution, also known as Fisher-Tippet type 1 distribution, is a good approximation of the population of such extreme values (U.S. Army Corps of Engineers, 2002).

In the present case, we are only interested in extreme wave height values, of long return period. To derive these, following the U.S. Army Corps of Engineers' (2002) recommendations, a time sample of monthly maxima of H_s is first extracted from the 20 year hourly time series; this yield $N = 240$ values.

A Gumbel distribution is curve fitted to these monthly maxima, and then used to predict (extrapolate) longer-term return period values. The Gumbel [1] cumulative probability distribution $F(x)$ of a variable x (e.g., extreme wind speed W (m/s) or significant wave height H_s) is defined as,

$$F(x) = \exp\left[-\exp\left(-\frac{x-B}{A}\right)\right] \qquad (0.1)$$

where, A is a scale parameter and B is a location parameter corresponding to the mode of the distribution. The standard deviation estimate, s_x, and mean, $\bar{x}$, of the sample of extreme values are related to these parameters by: $\bar{x} = B + A\gamma$; $s_x = 1.28255A$, with $\gamma = 0.5272$ being the Euler constant. Note these are (average) theoretical values assuming an ideal Gumbel distribution.
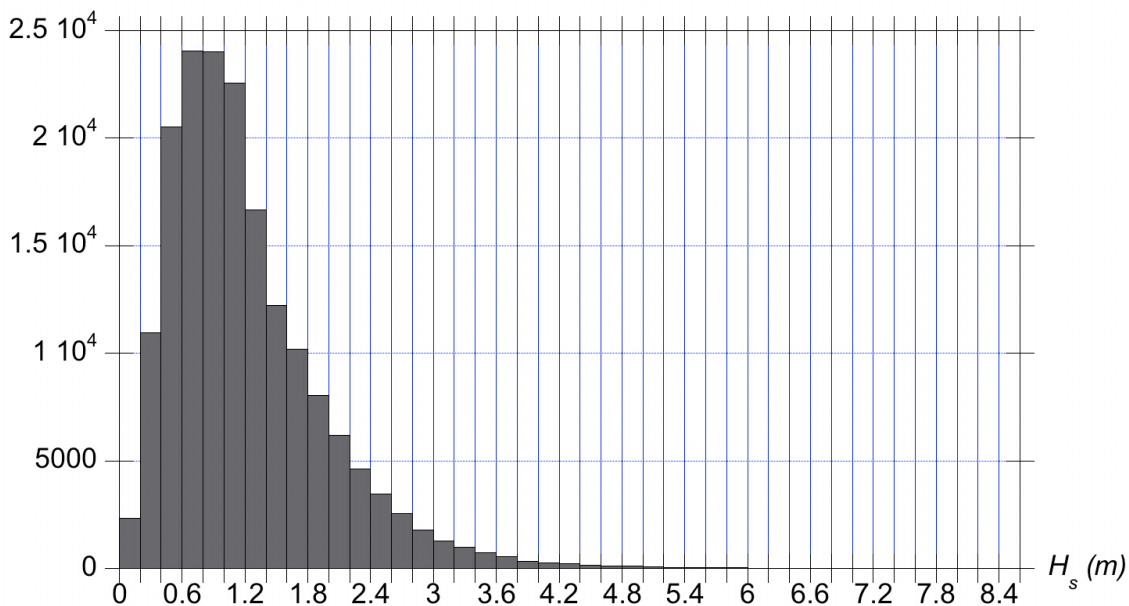
Figure 0.2 : Histogram (in count) of significant wave height at WIS station #101 (Fig. 1.2) over 1980-1999.

The return period, T_r (in years), of extreme events exceeding a certain threshold x_r is defined as,

$$T_r = \frac{1}{1 - F(x_r)} \qquad\qquad (0.2)$$

where the denominator is the probability of exceedance, or the probability that the extreme variable $x > x_r$.

In the sample of observed extreme values x_i, with $i = 1,\ldots, N$, ordered by decreasing magnitude, the probability that $x \le x_m$, the mth ordered variable is,

$$\widehat{F}(x_m) = 1 - \frac{m}{N+1} \qquad\qquad (0.3)$$

Using Eq. (0.3), one can plot events x_m versus their probability of occurrence expressed as $y_m = \ln(\ln \widehat{F}(x_m))$, or using the return period formula in Eq. (2.1.2), versus their return period expressed as, $y_r = \ln(\ln(1 - 1/T_r))$.

A linear curve fit of the form, $x = Ay + B$, then allows one to find the most representative values of Gumbel coefficients *(A, B)* for the given sample of extreme values. Once this is done, the Gumbel distribution can be used to predict the x value corresponding to a specified return period, longer than 20 years. As is customary in statistical inference, a 95 % confidence interval for extrapolated values is calculated and, in the present case, the upper confidence limit is used as a conservative extreme estimate.

Samples of $N = 240$ monthly extreme significant wave height and wind values were thus constituted based on the 20 year time series of hindcast WIS data, for a series of 30 degree directional sectors centered on 90, 120, 150, 180, 210, and 240 degrees clockwise from North. Curve fits were performed for each of these directional bins, as explained above. This provided six pairs of Gumbel coefficients, allowing extrapolation of extreme wind and wave directional data to 50, 75, and 100 year return periods, and calculating their upper 95% confidence limit. Figure 2.3 illustrates our methodology and results for extreme winds and significant wave heights, in the southern sector, located 180 deg. from North. The confidence limits appear in the figure in the form of extended hyperbolas, due to the logarithmic scale. We see that most of the data falls within the confidence limits, with only a few *outliers* in each case.

Extreme peak spectral wave periods, T_p, are estimated from predicted extreme significant wave height, H_s, by assuming these correspond to fully developed sea conditions, according to the following formula [4],

$$T_p = 15.66\sqrt{\frac{H_s}{g}}$$

(0.4)

(a)

(m/s)

(b)

H_s (m)
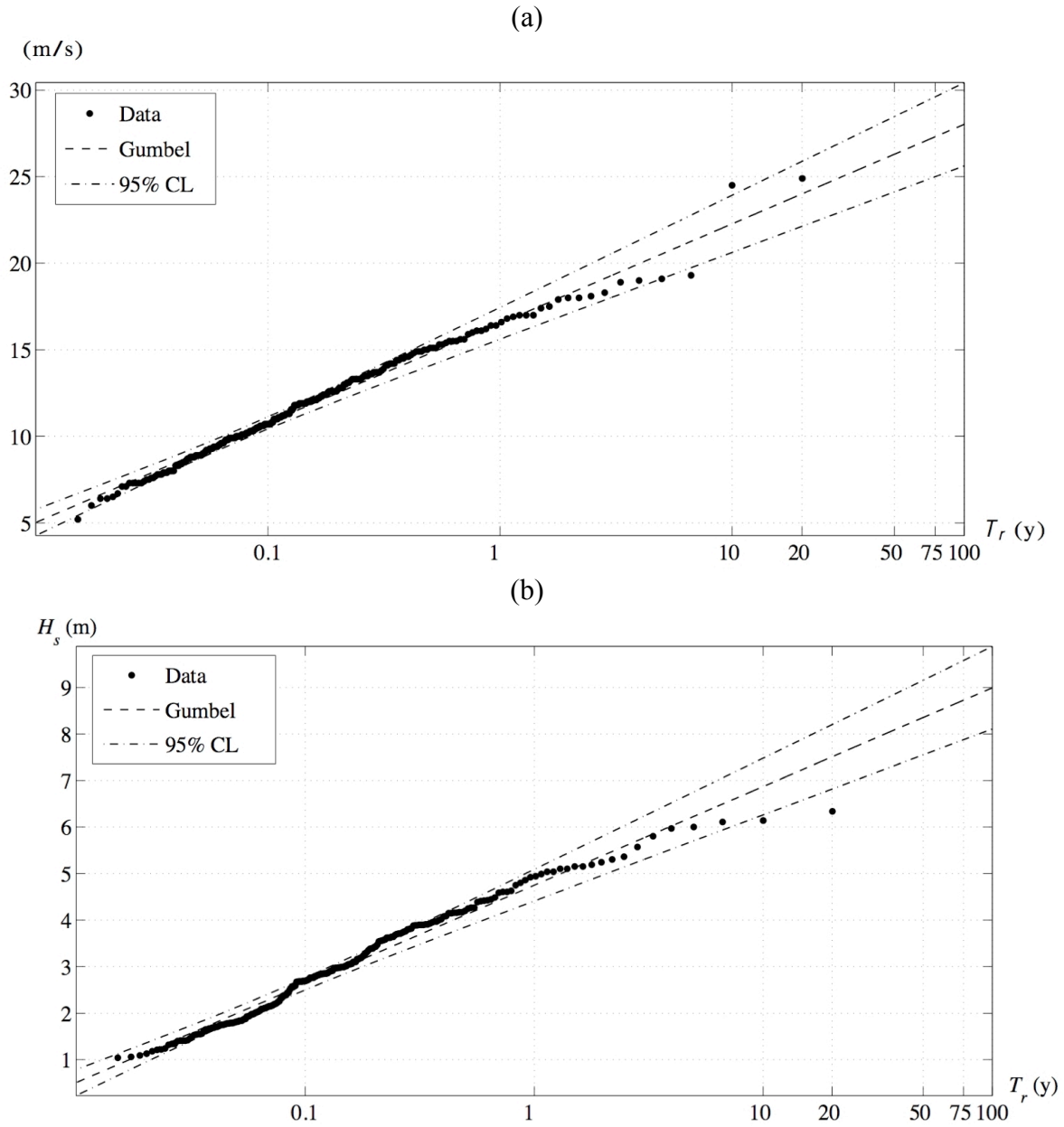
Figure 0.3 : Gumbel probability plot and curve fit for extreme: (a) wind speed; and (b) significant wave height, as a function of return period T_r , based on monthly extrema hindcast at WIS station #101, over 1980-1999, in the 30 deg. sector centered on the Southern direction (i.e., 180 deg. from North).

Tables 2.1 and 2.2 give detailed results of analyses for the wave and wind parameters, respectively, as a function of storm return period and direction.

Extreme wind speeds and wave heights (and the limits of the 95% confidence intervals for each return period) are used to formulate input wave spectra for STWAVE simulations, as presented in Section 3.

Direction from North	Return Period (yr)	H_s mean (m)	T_p mean (s)	H_s lower 95% (m)	T_p lower 95% (s)	H_s upper 95% (m)	T_p upper 95% (s)
90.0	100	8.8	14.8	7.8	14.0	9.8	15.7
	75	8.5	14.6	7.6	13.7	9.5	15.4
	50	8.1	14.2	7.2	13.4	9.0	15.0
	20	7.2	13.4	6.4	12.7	8.0	14.1
120.0	100	8.6	14.7	7.7	13.9	9.6	15.5
	75	8.4	14.5	7.5	13.7	9.3	15.2
	50	8.0	14.1	7.1	13.3	8.8	14.8
	20	7.1	13.3	6.4	12.6	7.8	14.0
150.0	100	8.9	14.9	7.9	14.1	9.8	15.6
	75	8.6	14.6	7.7	13.9	9.5	15.4
	50	8.2	14.3	7.4	13.6	9.0	15.0
	20	7.3	13.5	6.6	12.8	8.0	14.2
180.0	100	9.0	15.0	8.1	14.2	9.9	15.7
	75	8.7	14.8	7.9	14.0	9.6	15.5
	50	8.4	14.5	7.6	13.7	9.2	15.1
	20	7.5	13.7	6.8	13.1	8.2	14.3
210.0	100	8.8	14.8	7.9	14.1	9.7	15.6
	75	8.6	14.6	7.7	13.9	9.4	15.3
	50	8.2	14.3	7.4	13.6	9.0	15.0
	20	7.3	13.5	6.6	12.9	8.0	14.2
240.0	100	8.3	14.4	7.4	13.6	9.1	15.1
	75	8.0	14.1	7.2	13.4	8.8	14.9
	50	7.6	13.8	6.9	13.1	8.4	14.5
	20	6.8	13.1	6.1	12.4	7.5	13.7

Table 2.1: Extreme wave parameters (with upper and lower 95% confidence intervals), as a function of storm return period and direction, based on analyzing 20 years of data (1980-1999) at WIS station 101.

Direction	Return Period (yr)	U mean (m/s)	U lower 95% (m/s)	U upper 95 % (m/s)
90	100	31.0	28.0	34.0
	75	30.1	27.2	33.0
	50	28.9	26.1	31.6
	20	26.1	23.7	28.4
120	100	29.7	26.8	32.5
	75	28.8	26.1	31.5
	50	27.6	25.1	30.2
	20	25.0	22.8	27.1
150	100	27.8	25.3	30.3
	75	27.0	24.6	29.4
	50	26.0	23.7	28.2
	20	23.6	21.7	25.6
180	100	28.0	25.6	30.4
	75	27.3	25.0	29.6
	50	26.3	24.1	28.5
	20	24.0	22.1	25.9
210	100	29.2	26.8	31.7
	75	28.5	26.1	30.9
	50	27.5	25.2	29.7
	20	25.1	23.2	27.0
240	100	31.3	28.5	34.0
	75	30.5	27.8	33.1
	50	29.3	26.8	31.8
	20	26.7	24.5	28.9

Table 2.2: Extreme wind parameters (with upper and lower 95% confidence intervals), as a function of storm return period and direction, based on analyzing 20 years of data (1980-1999) at WIS station 101.

Return Period (yr)	Water level (m) at MHHW
20	3.706
50	4.376
75	4.416
100	4.446

Table 2.3: Extreme storm surge events in study area, from Ref. [5]

2.2 Storm Surge

Storm surge values in the study area were found from U.S. Army Corps of Engineers tidal flood profiles [5], and are reported in Table 2.3. These values are also used as input for STWAVE simulations. Note, the interest here is to determine the impact of storm surge on the wave field and specifically how increases in water depths alter wave heights in this study area, rather than, e.g., calculating coastal inundation.
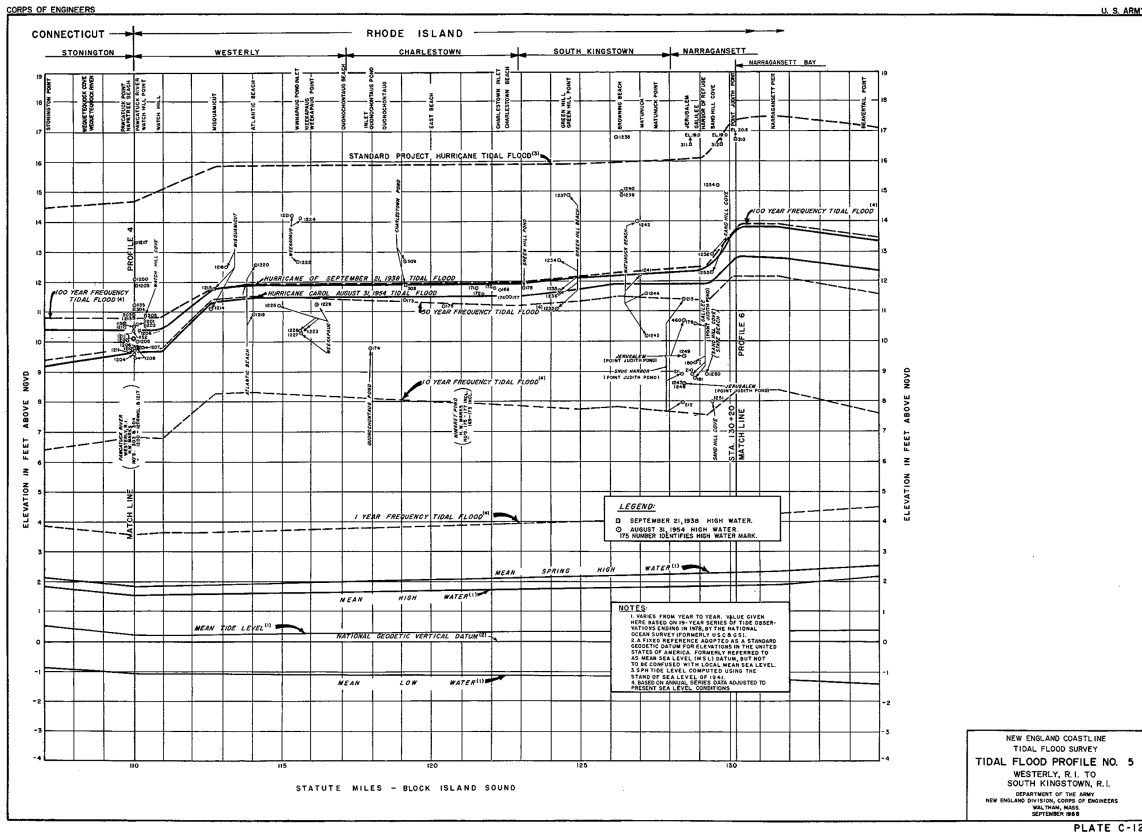

Figure 0.4 : Tidal flood profile; matchline #123 was used for storm surge values.

Using matchline #123 on Fig. 2.4, predictions for storm surge at certain return intervals are provided. By linearly interpolating, storm surge values for the 25- and 75-year return period cases were found.

3 Wave Modeling

3.1 Model governing equations and numerical methods

Propagation of incident wave climates for various return periods and directions, obtained from WIS station #101 data as detailed in Section 2, combined with corresponding storm surges, is simulated using the wave model STWAVE (version 4.0), developed and maintained by the US Army Corps of Engineers [2]. STWAVE is a steady-state spectral model, based on a wave action conservation equation. The model is capable of simulating wind forcing (fetch growth), wave-current interactions, and breaking dissipation (both surf zone and white capping). Details on STWAVE are provided in Appendix A.

Note that the main difference between STWAVE and operational wind wave models such as WAVEWATCH III or SWAN is that it assumes a steady-state wave spectrum (i.e., sea state) during coastal wave propagation and transformations. Hence only spatial variations are considered (see Eq. A.5 in Appendix), as a function of depth variations and currents, which is acceptable here since we only consider short distances of propagation.

3.2 Input directional wave spectrum

STWAVE requires a full directional wave energy density spectrum as input on the offshore boundary, while we only have significant wave height and peak spectral period values for each selected direction and return period (Table 2.1) and corresponding wind (Table 2.2).

Hence, the directional wave frequency spectrum is formulated as a standard semi-empirical spectrum, here, the Bretschneider-Mitsuyasu frequency spectrum multiplied by a standard cosine-squared directional spreading [2],

$$S(f,\theta) = 0.257 \frac{H_{1/3}^2}{T_{1/3}^4} f^{-5} \exp\left\{-1.03\left(T_{1/3}f\right)^{-4}\right\} G(f,\theta)$$

$$T_{1/3} = \frac{T_p}{1.05} \tag{3.2.1}$$

where, T_p is the peak spectral period (s), $H_{1/3}$ and $T_{1/3}$ are significant wave height (m) and period (s), respectively, and f is *the* frequency (Hz), with

$$G(f,\theta) = G_0 \cos^{2s}\left\{\frac{\theta - \theta_p}{2}\right\} \tag{3.2.2}$$

and,

$$s = \begin{cases} s_{\max}\left(\dfrac{f}{f_p}\right)^5 & f \leq f_p \\[2em] s_{\max}\left(\dfrac{f}{f_p}\right)^{-2.5} & f > f_p \end{cases} \qquad \text{with} \qquad s_{\max} = 11.5\left(\dfrac{g}{2\pi W f_p}\right)^{2.5} \qquad (3.2.3)$$

where θ denotes a wave component direction, θ_p is the spectral peak direction, W is the wind speed (m/s) at 10 m above sea level, and coefficient G_0 is such that the definite integral of the spreading function over its entire angular domain is equal to 1.
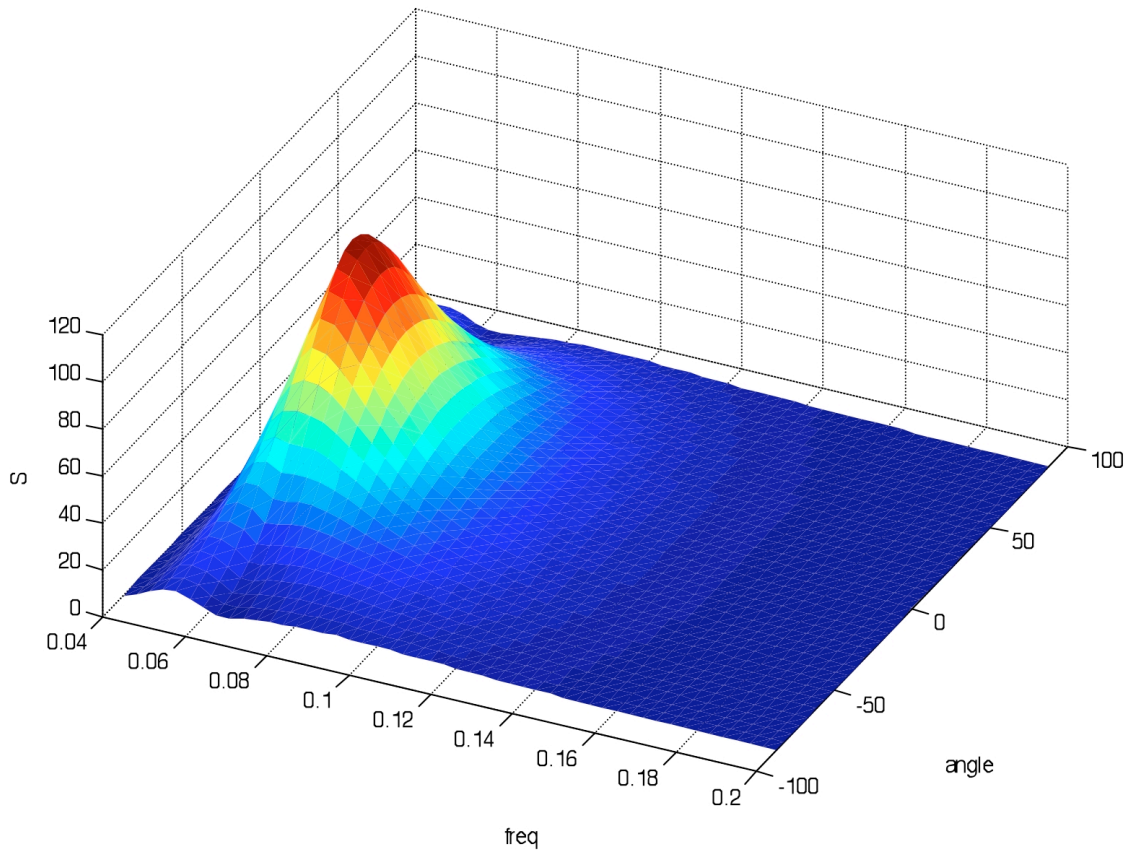
Figure 0.1 : Example of Bretschneider-Mitsuyasu directional frequency spectrum used as input to STWAVE, for T_p = 15.7 s, $H_{1/3}$ = H_s = 9.9 m, θ_p = 30 deg., and W = 30 m/s.

A standard frequency vector ranging linearly from 0.04 to 0.2 Hz is used to discretize the frequency axis in most STWAVE simulations, for both input and calculated spectra, over the STWAVE model grid. Fifty equally-spaced frequency bins are used, along with 35 directional bins (5 degree spacing). The input values for specific spectra, $H_{1/3} = H_s$, T_p, θ_p, and W, are obtained from the various earlier estimates of extreme wave conditions (see Section 0).

Fig. 3.1 shows an example of input wave spectrum.

4 Results of Wave Simulations for Block Island Sites

4.1 Computational domains for Block Island sites

The STWAVE computational domains are designed to maximize their size and resolution relative to the region of interest, while keeping computational costs reasonable. Considering the sites under consideration, adjacent to Block Island (Fig. 1.1), and the computing size/cost limitations in STWAVE, three separate model domains were generated for the purpose of this study.

Figure 0.1 : Bathymetry (m) near and around Block Island used in STWAVE, and extent of first computational domain

Bathymetric features (NOAA Electronic Navigation Charts (ENC)), which might have a significant effect on wave transformation in the considered region, have been included in each computational domain. Table 3.1 gives main model parameters (grid size and

number of grids in each direction) for these domains. The domains are shown in Figs. 4.1, 4.2, and 4.3. These cover areas ranging from 616 to 978 km^2.

Domain	Western Boundary Long. W	Eastern Boundary Long. W	Southern Boundary Lat. N	Northern Boundary Lat. N	Grid size (m)	Cells W->E	Cells S->N	Offshore boundary
1	-71.75	-71.40	40.95	41.25	50	588	665	east
2	-71.75	-71.50	41.00	41.25	50	419	588	south
3	-71.85	-71.50	41.00	41.25	50	555	588	south

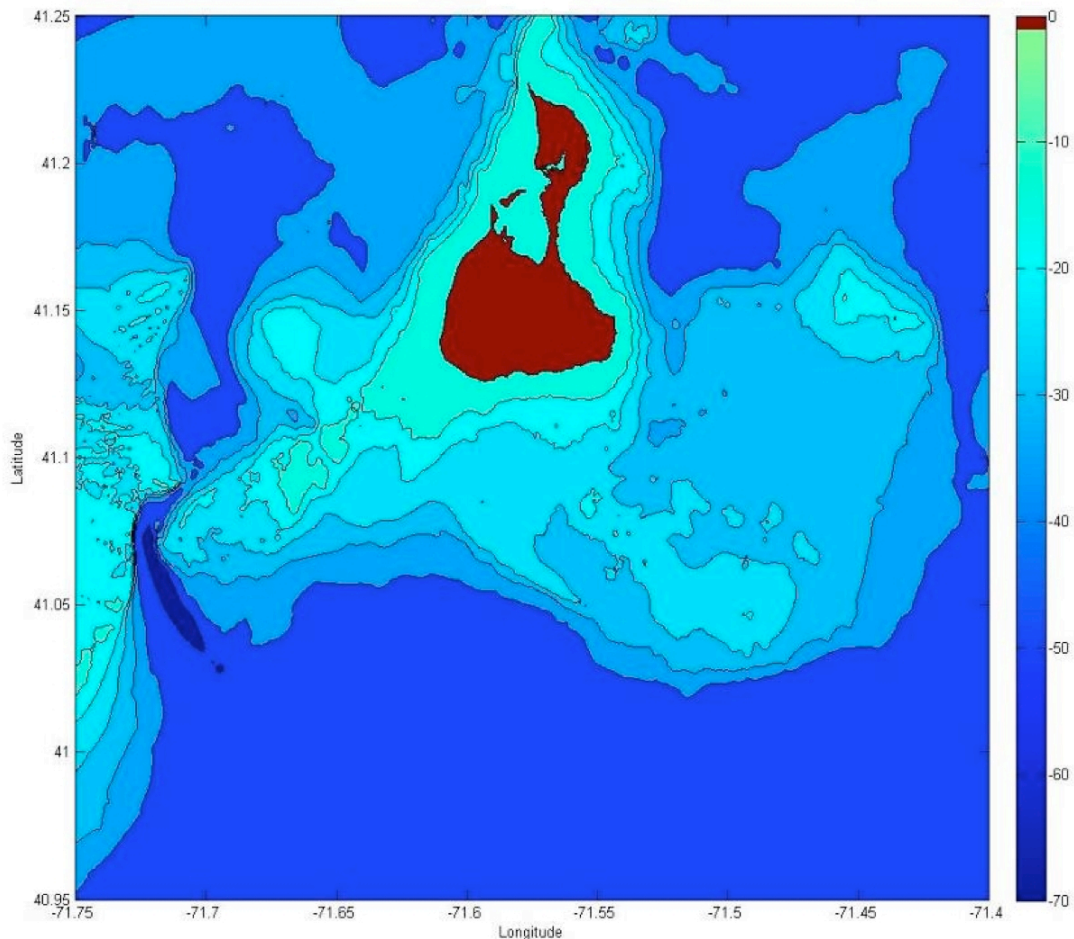**Table 4.1: Parameters for three main computational domains used in STWAVE**
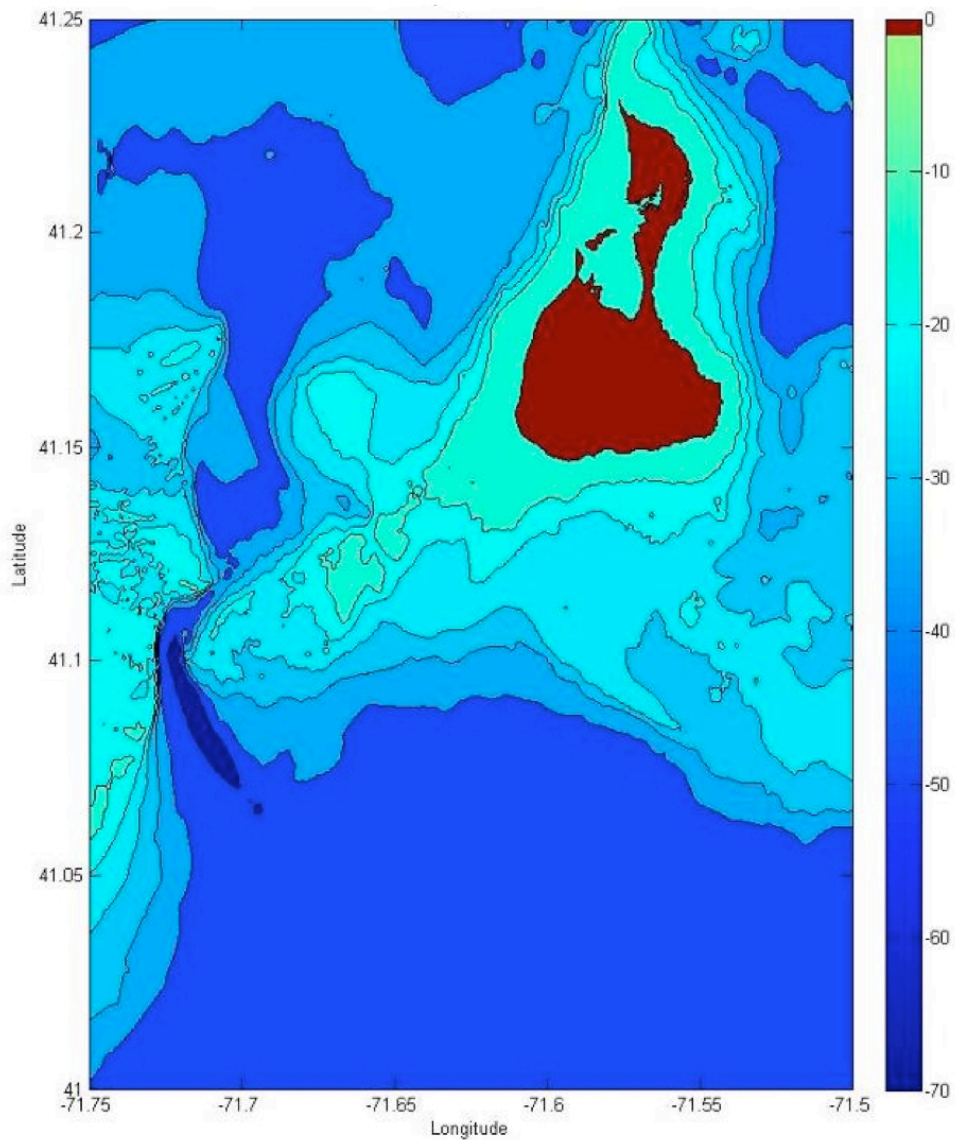

Figure 0.2 : Bathymetry (m) near and around Block Island used in STWAVE, and extent of second computational domain

The first computational domain (Fig. 4.1) is used for simulating waves originating from the 90° and 120° sectors. The domain encompasses an area of 978 km^2 (29.4 km (W-E) x 33.25 km (S-N)), with the offshore boundary in STWAVE defined as the eastern boundary of the domain. The grid size is 50 m. It should be noted that, while WIS station #101 is not spatially near the eastern boundary of this domain, the analysis of other WIS stations closer to this boundary showed little variation in extreme wave parameters.

The second computational domain (Fig. 4.2) is used for simulating spectra for waves from 210°-150°. It encompasses an area of 616 km^2 (20.95 km (W-E) x 29.4 km (S-N)), with the offshore boundary in STWAVE defined as the southern boundary of the domain. The grid size is 50 m. This boundary is chosen to match the latitude of WIS station #101. Since incident wave climates are estimated from the hindcast data at this WIS station, this selection typically ensures that the wave climate at the start of the simulation is accurate. This domain, the smallest of the three, is used for the majority of simulations.

The third computational domain (Fig. 4.3) is used for simulating spectra for waves from 240°. It encompasses an area of 816 km^2 (27.75 km (W-E) x 29.4 km (S-N)), with the offshore boundary in STWAVE defined again as the southern boundary of the domain. The grid size is 50 m. Because of the direction of this simulation, it was deemed necessary to include more of the bathymetry west of Block Island. Accordingly, domain two was extended westward.
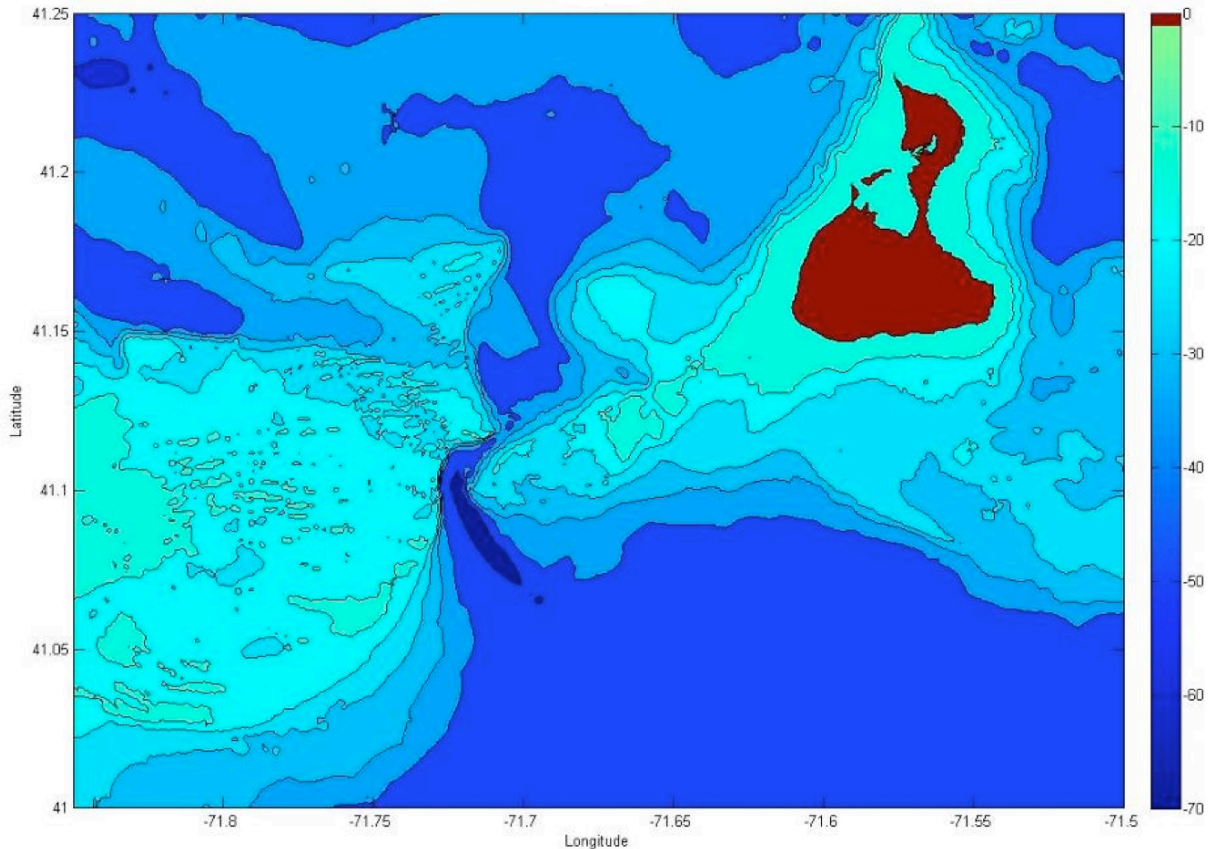
Figure 0.3 : Bathymetry (m) near and around Block Island used in STWAVE, and extent of third computational domain.

4.2 Simulation results

Although simulations were done for multiple wave directions, a leading angle of incidence of 180° (waves arriving from the south), and to a lesser extent 90°, consistently provided the worst-case scenarios in the region of interest.

The worst-case scenario (waves from the south) significant wave heights are plotted in Figs. 4.4, 4.5, 4.6, and 4.7, for the 20, 50, 75, and 100 year storms, respectively. The plots show colored renditions of the significant wave height within the study domain. Note the same height scale is used on each of the figures.

Figure 0.4 : Worst-case scenario significant wave height for 20 year storm (axis in m). Incident conditions : H_s = 8.2 m, T_p = 14.3 s, W = 25.9 m/s, and 180° direction.

Qualitatively, the canyon (approximately 71.71^{o}W, 41.05^{o}N) in the southwestern section of the study area and the shoal (approximately 71.66^{o}W, 41.08^{o}N) northeast of it, appears to provide some sheltering for the area west of Block Island, yielding significant wave heights of 6-8 m across most of the region for the 100 year storm (Figs. 4.7). South and east of the island, however, no such protection exists and large significant waves prevail, some in excess of 10 m for the 100 year storm. For the shorter return period waves (Figs. 4.4, 4.5, and 4.6) the wave amplitudes are reduced but the pattern remains the same as for the 100 year case.
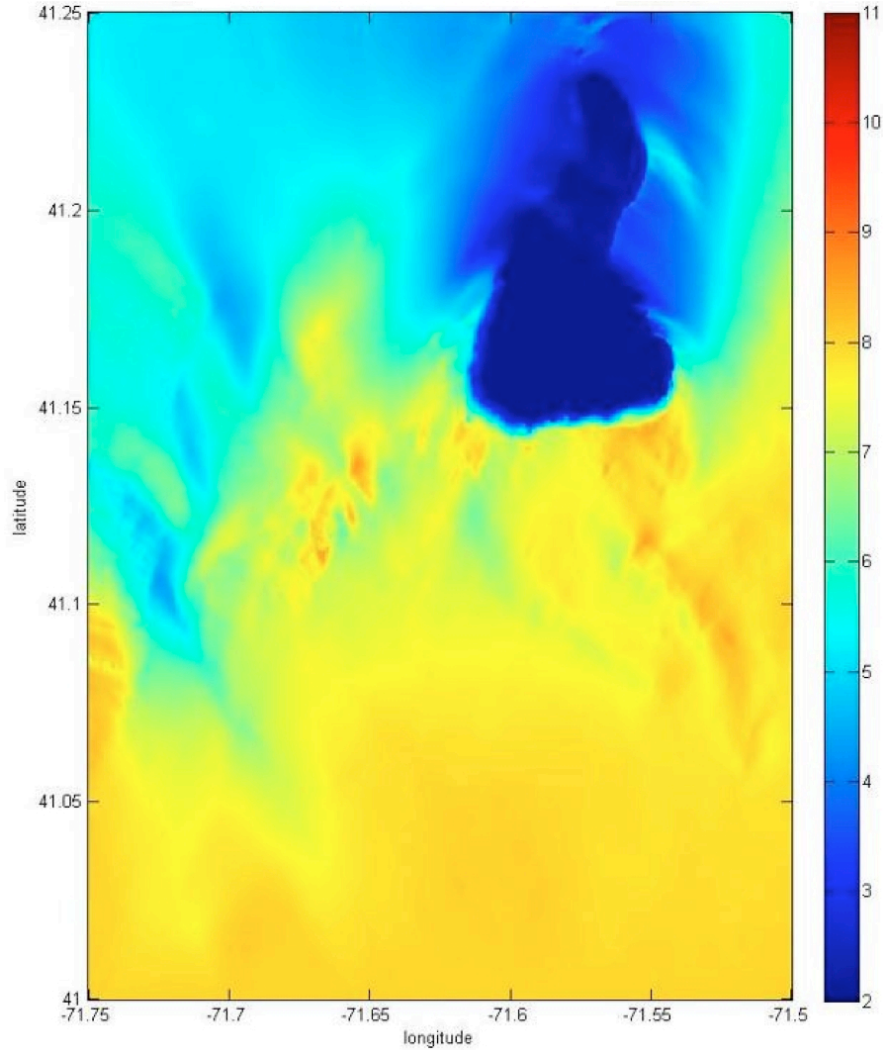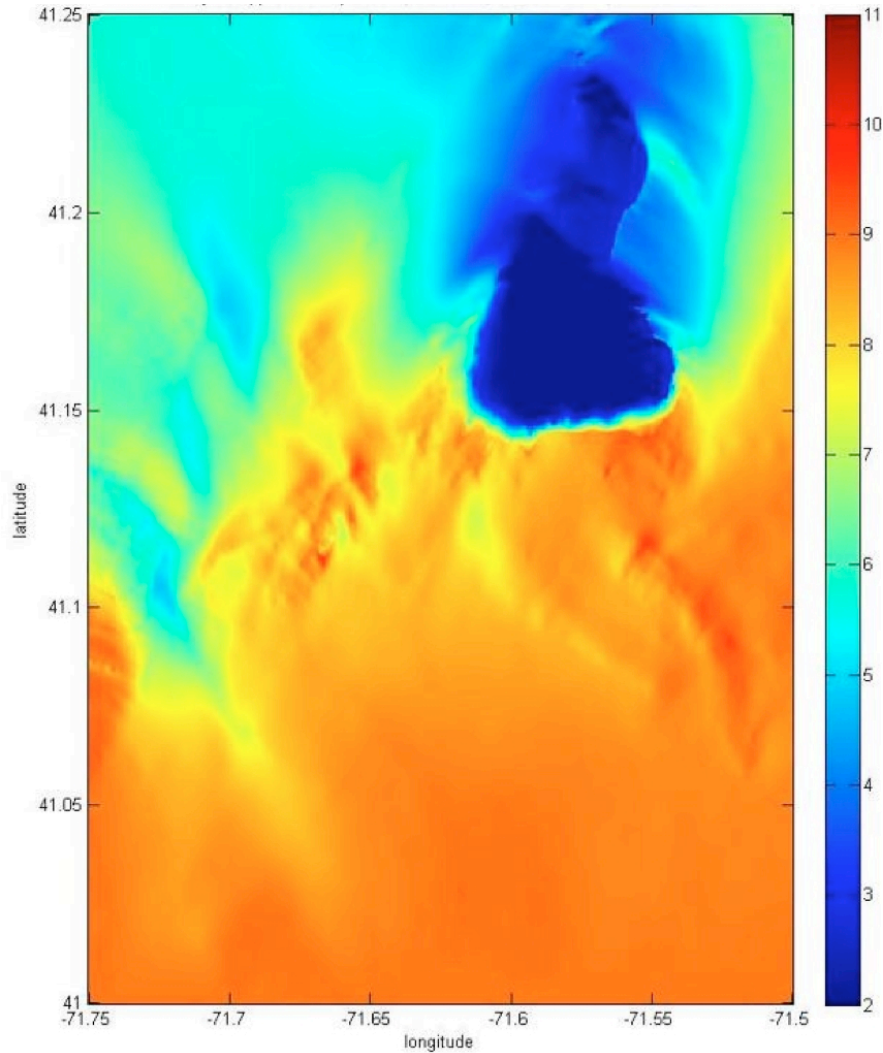
Figure 0.5 : Worst-case scenario significant wave height for 50 year storm (axis in m). Incident conditions : H_s = 9.2 m, T_p = 15.1 s, W = 28.5 m/s, and 180° direction.

Comparing simulated variations in significant wave height across different return periods reveals that the above sheltering effects also limit wave heights west of Block Island to some degree. South of the island, the 20 year return period significant waves (Fig. 4.4) are about 2.5 m smaller than those in the 100 year scenario (Fig. 4.7). North of the canyon and shoal, however, the disparity in wave height among various return periods is generally less than 1 m. This can be explained through the depth-limitation of a given wave height, i.e. shallow depth induces wave breaking, dissipating energy continually until wave height has reduced below the breaking limit. This explanation is also confirmed by the fact that, beyond a transition zone, wave height is approximately the same for each return period.

The above results are consistent with expectations and confirm that wave climate should be considered as a determining factor for the siting of a wind farm off of Block

Island. In particular, the reduced wave height west of the island marks this area as a much more desirable option than south or south-east of the island, based on the extreme wave height aspect only.
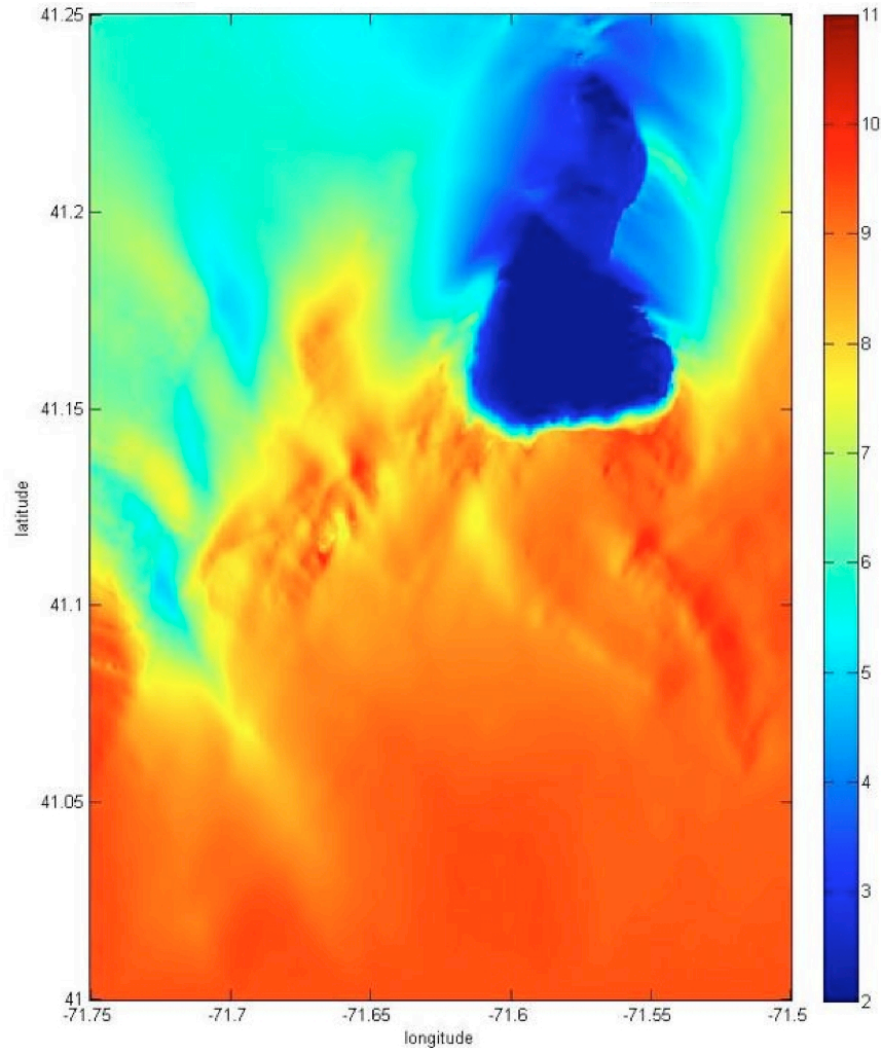
Figure 0.6 : Worst-case scenario significant wave height for 75 year storm (axis in m). Incident conditions : H_s = 9.6 m, T_p = 15.5 s, W = 29.6 m/s, and 180° direction.

Figure 4.8 shows simulation results for the worst-case scenario for waves from the east. We note that large amplitude waves propagate to the shoreline with some evidence of a small amplification to the south and southeast of Block Island. Wave heights are dramatically lower in the lee of the island and landward of the shoal area to the SW of the island.

**Figure 0.7 : Worst-case scenario wave height for 100 year storm (axis in m),
180 deg. incidence. Incident conditions : H_s = 9.9 m, T_p = 15.7 s, W = 30 m/s,
and 180° direction.**

4.3 Sensitivity to bathymetric resolution

In this section, we verify the accuracy of STWAVE simulations with respect to the
bathymetric resolution, defined as the size of grid cells in the computational domain.
Three cases were tested, with different grid cell sizes: 30 m for the highest resolution; 50
m for the intermediate case (default value used in standard extreme analysis simulations
presented above); and 70 m for the lowest resolution case.

Figures 4.9 (30 m), 4.10 (50 m) , and 4.11 (70 m) show results for the three
bathymetric resolutions for 9 m, 15 s waves from the south with winds of 30 m/s. We see
negligible differences in significant wave height across the domain for all three cases. It

can therefore be concluded that the 50 m bathymetric resolution used in earlier simulations adequately represents the study area and does not cause significant errors in wave predictions.
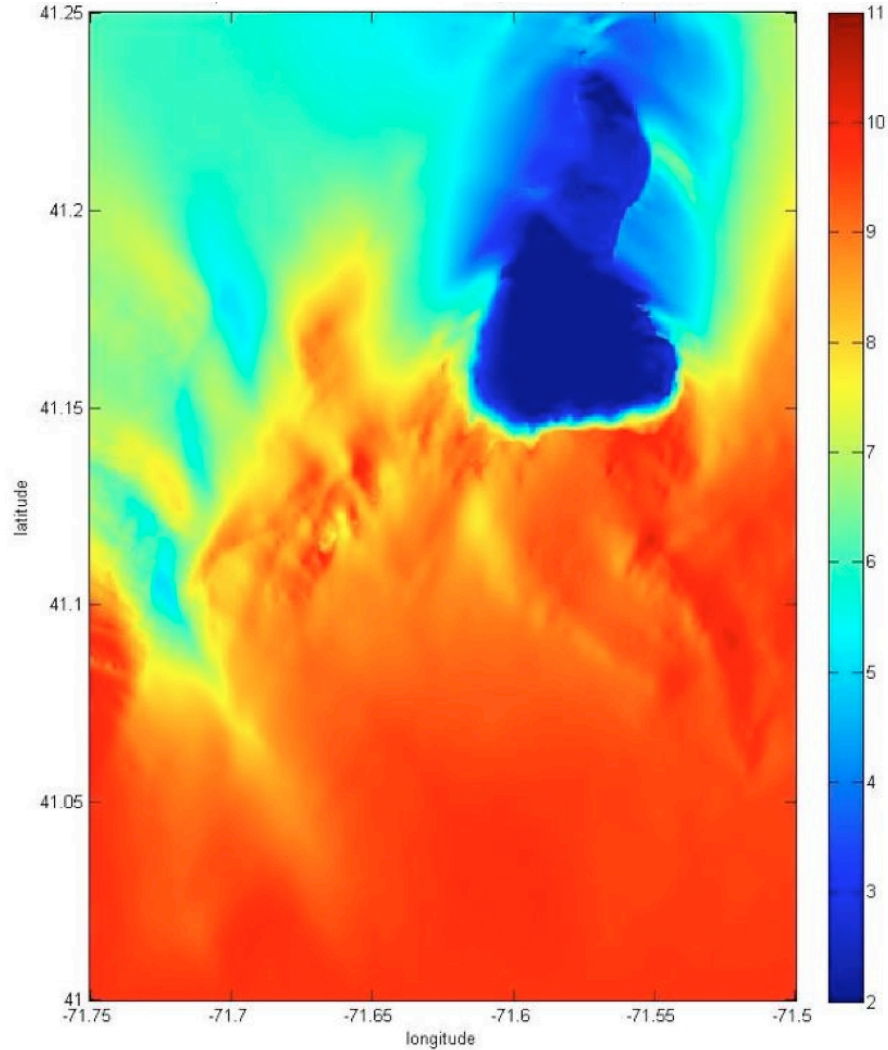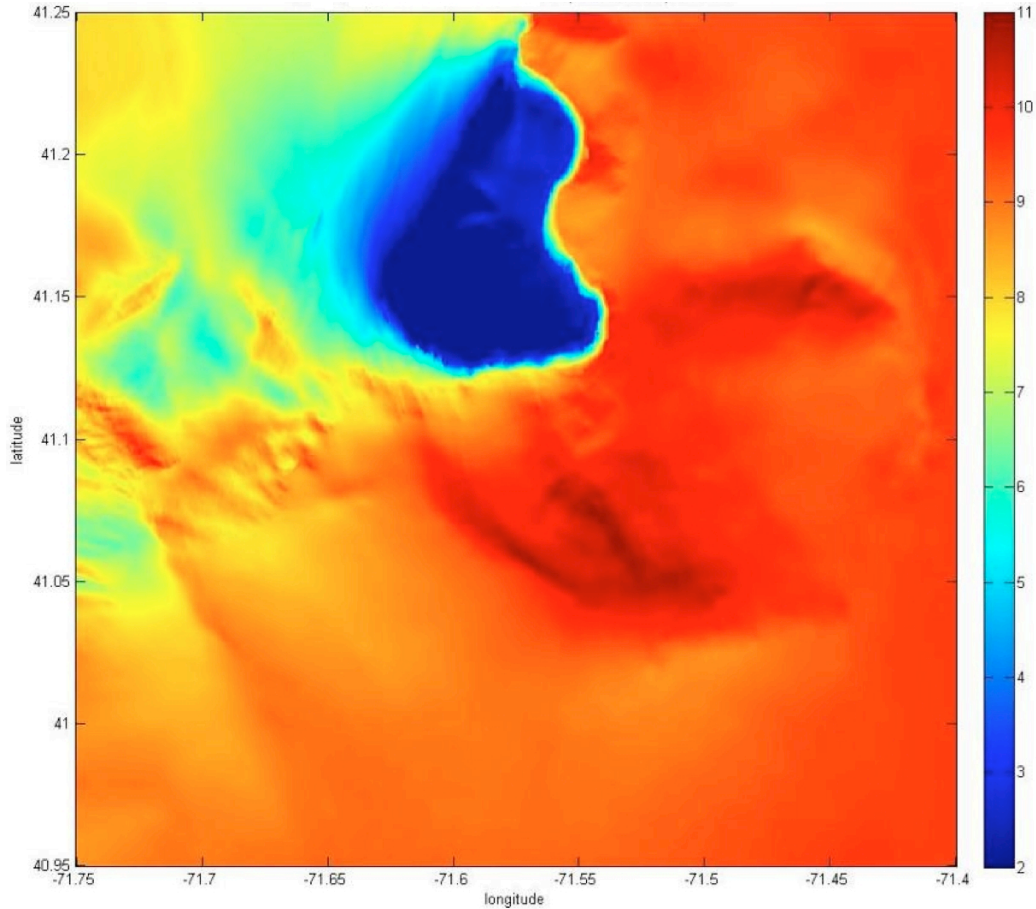

Figure 0.8 : Worst-case scenario wave height for 100 year storm (axis in m), 90 deg. incidence. Incident conditions : H_s = 9.8 m, T_p = 15.7 s, W = 34 m/s, and 90° direction.

4.4 Sensitivity to domain size

   In this section, we verify the accuracy of STWAVE simulations with respect to the extent of the computational domain. The latter can have an effect if salient aspects of the bathymetry that might otherwise influence wave transformation processes, such as refraction, are not included in the domain.

Figure 0.9 : Significant wave height (axis in m), for 30 m bathymetric resolution

Figure 0.10 : Significant wave height (axis in m), for 50 m bathymetric resolution

Figure 0.11 : Significant wave height (axis in m), for 70 m bathymetric resolution
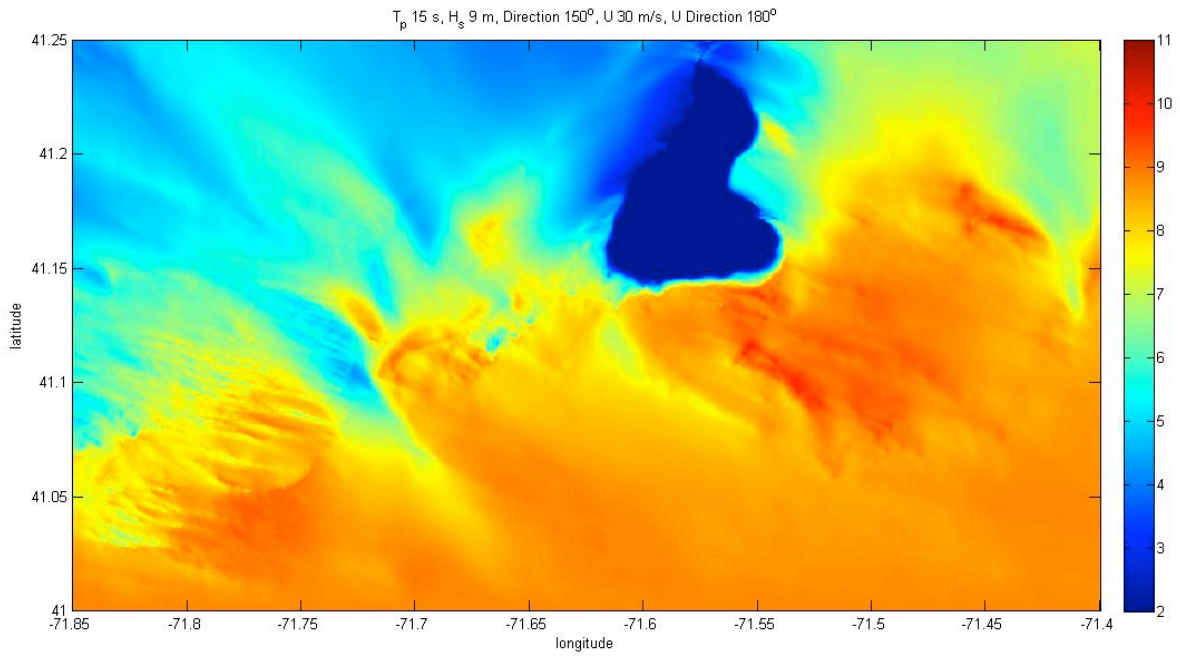
Figure 0.12 : Significant wave height (axis in m) for wide domain.

In these tests, the southern boundary of the computational domain is kept at around the location of the WIS station #101 (i.e., 41° lat.), and the longitudinal extent of the domain is gradually increased. Three cases were 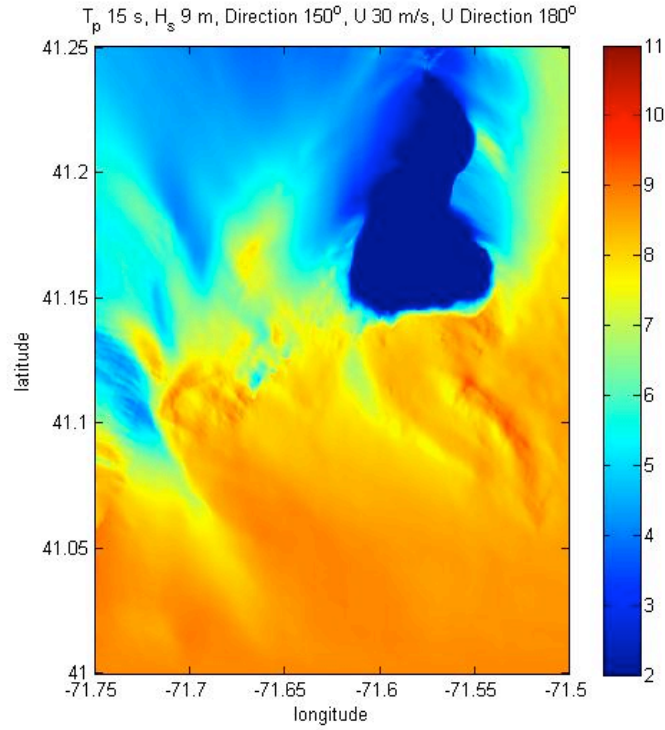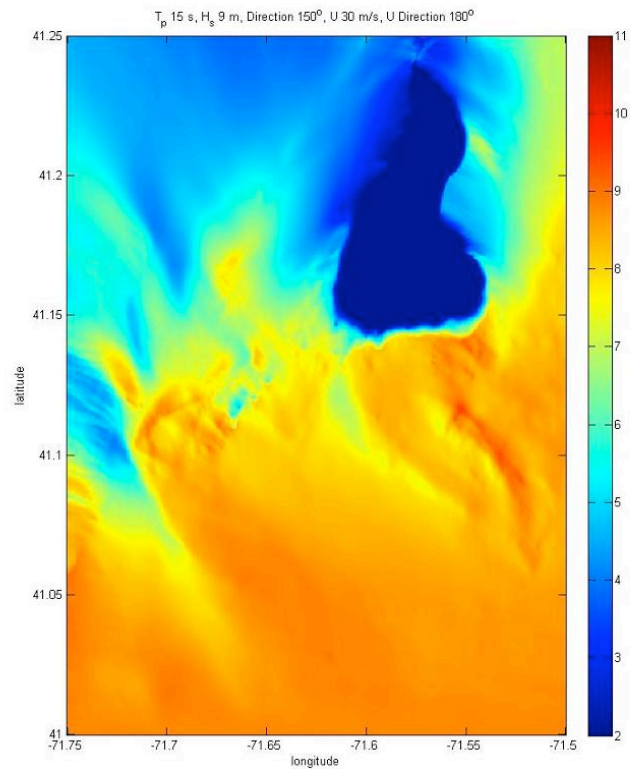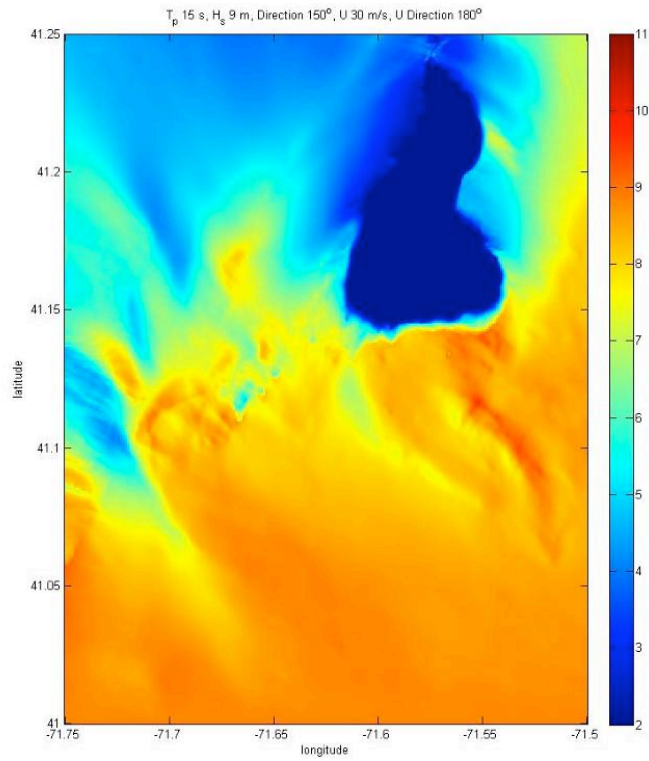tested, 71.85-71.40^o W (wide domain), 71.75-71.50^o W (standard used in simulations), and 71.72-71.53^{o}W (narrow domain). Simulations were performed for a 9 m significant wave height, 15 s peak spectral period from 150 deg., with a 30 m/s wind from the south.

Results for the two wider domains in Figs. 4.12 (wide) and 4.13 (mid) show small variations in simulated significant wave height. Results for the narrower domain in Fig. 4.14 (narrow), however, show significant differences, particularly in the region far west of Block Island, where wave heights are larger. This is likely due to the absence of effects of the complex bathymetry around the canyon mentioned earlier. These simulations show that results are independent of domain size as long as the domain is larger than the medium case (Fig. 4.13), but are significantly impacted for the narrow case (Fig. 4.14). The simulation cases presented in Section 3 used the medium domain and hence should give reliable estimates.
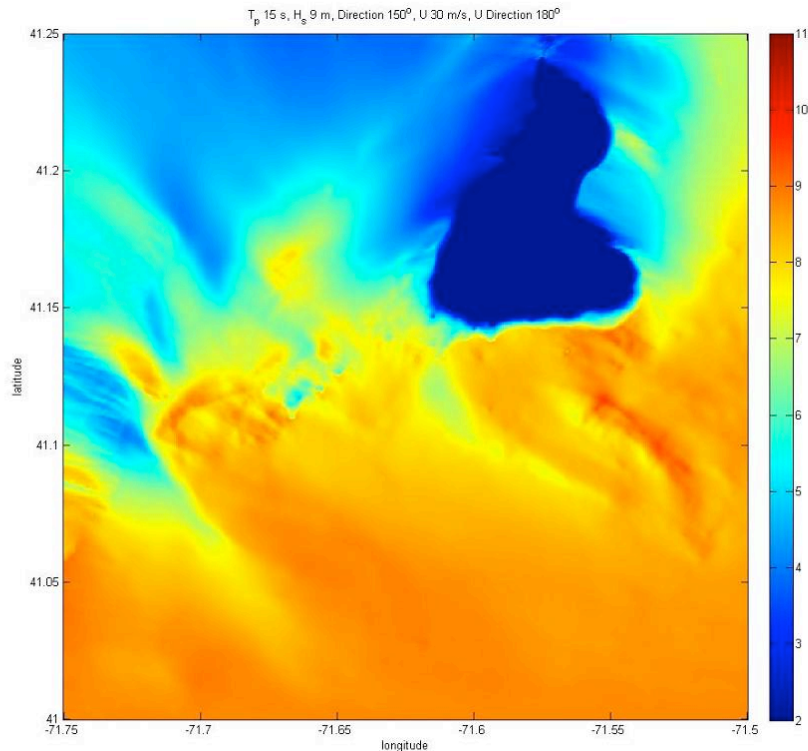
Figure 0.13 : Significant wave height (axis in m) for medium (standard) domain.
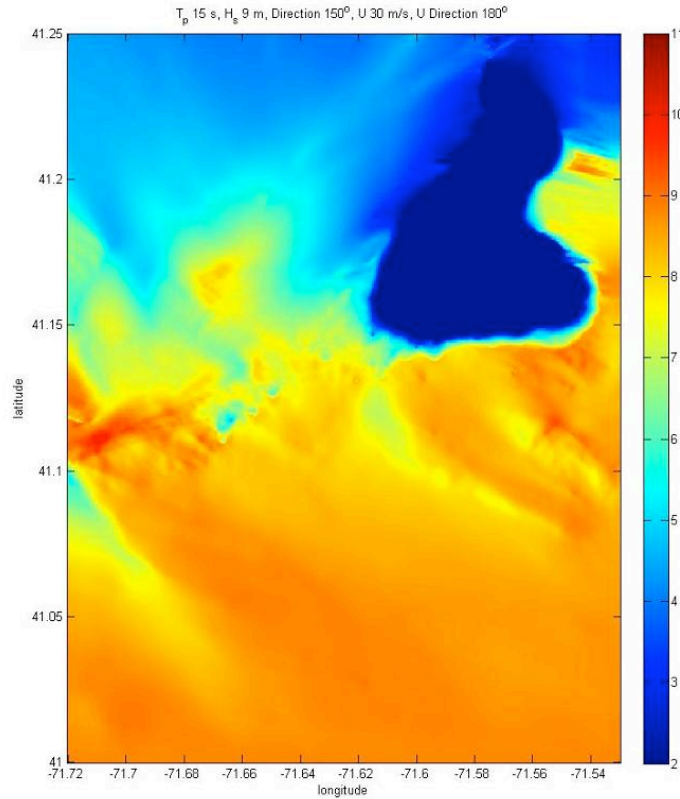
Figure 0.14 : Significant wave height (axis in m) for narrow domain.

4.5 Sensitivity to spectral resolution

In this section, we verify the accuracy of STWAVE simulations with respect to the frequency resolution of the wave spectrum used as input to the model.

The latter must accurately represent the shape of the incident wave spectrum, as well as the effects of subsequent wave transformations, as these are both related to frequency. As before, three cases were evaluated: 20 frequency bins (low resolution), 50 frequency bins (medium resolution; the standard value used in extreme simulations), and 80 frequency bins (high resolution). As before, simulations were performed for a 9 m significant wave height, 15 s peak spectral period from 150 deg., with a 30 m/s wind from the south.

The difference in results, shown in Figs. 4.15, 4.16 and 4.17, for low, medium, and high frequency cases, respectively, is negligible. While the low resolution case shows larger wave heights in the region southeast of Block Island, it is also very similar to results of the 80 frequency bin case.
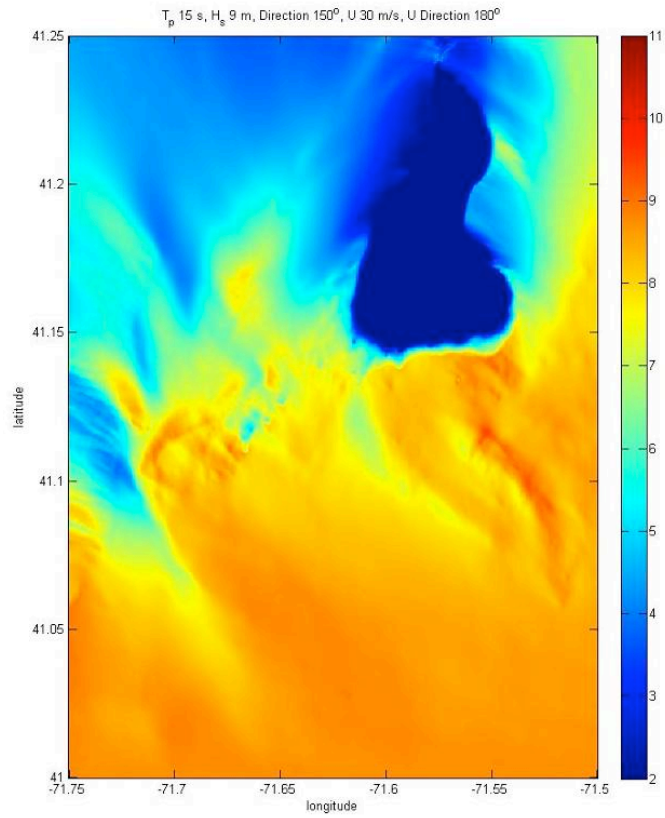
Figure 0.15 : Significant wave height (axis in m) for low frequency resolution.

Figure 0.16 : Significant wave height (axis in m) for medium (standard) frequency resolution.

Figure 0.17 : Significant wave height (axis in m) for high frequency resolution.

5 Conclusions

The objectives of this study were first to obtain estimates of sea state conditions associated with extreme storm events, for return periods of 20, 50, 75, and 100 years in the coastal region immediately to south of Block Island, and then to use these estimates as input into a numerical wave simulation model, that provide estimates of the extreme wave climate for the region.
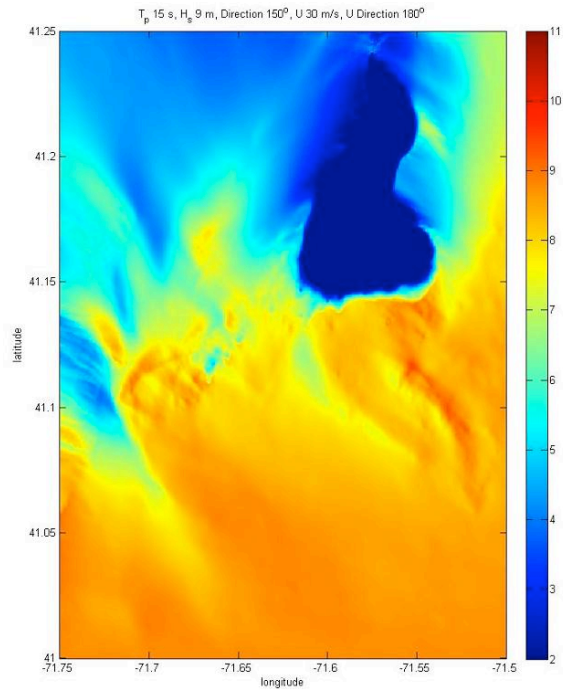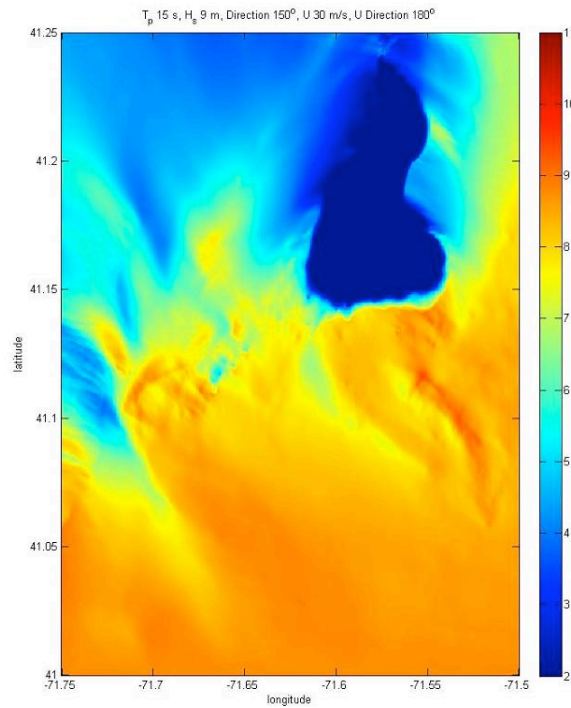
The wave estimates were calculated based on a statistical analysis of 20 years of hindcast wave (and wind) data, available from the nearby WIS station #101. These were converted into standard directional wave frequency spectra and used as input to STWAVE, a steady-state spectral wave model. The outputs of such simulations were significant wave height, peak spectral period, and directional spread, as well as locations of actively breaking waves.

Wave climates were found to vary strongly geographically, with the significant wave heights west of Block Island typically being 2-3 m less than that south of Block Island (9 m). Similarly, the difference in wave height for each return period is smaller in the region west of the island due to depth-limiting shallow shoals that cause breaking and dissipation (i.e., bathymetric filtering).

Thus, as far as exposure of wind turbine structures to extreme waves, the waters surrounding Block Island cannot be considered homogeneous in terms of potential for development of offshore wind farms. The difference in wave climates west and south of the island represents a key distinguishing factor, with the more desirable area in this respect being southwest and west of the island.

A sensitivity analysis of simulation results to grid size and frequency showed negligible effects. Results only showed a small sensitivity to the lateral extent of the computational domain and that the width must be sufficient to capture effects of salient bathymetric features. This was the case for the standard domains used in these simulations.

The STWAVE simulations, within the assumptions of the model (see Appendix A), may therefore be considered representative of actual extreme storm wave conditions that can be expected at the site, during the typical life time of wind farm.

Finally note that this entire study relies on the relevance of the wave (and wind) data from the WIS station #101. Indeed, WIS provided 20 years (1980-1999) worth of hourly hindcast data for wind speed and direction, significant wave height, and peak spectral period. Hence, the present study and results depend upon the relevance of this time series to describe the present day wave climate around Block Island. In particular no effect of climatic change that may have occurred over the past 10 years, and of any future changes that might occur, on extreme wave parameters is included.

6 References

[1] Goda Y, 2000. Random seas and design of maritime structures, in Advanced series of Ocean Engineering, Vol. 15. Published by World Scientific, 443p.

[2] Smith, Jane McKee, Sherlock, Ann R., & Resio, Donald T. *STWAVE: Steady-State Spectral Wave Model User's Manual for STWAVE, Version 3.0.* Coastal and Hydraulic Laboratory, U.S. Army Engineer Research and Development Center. February, 2001.

[3] U.S. Army Corps of Engineers, 2004. Coastal and Hydraulics Laboratory Wave Information Studies, ERDC Waterways Experiment Station, Vicksburg, MS.

[4] U.S. Army Corps of Engineers, 2002. Coastal Engineering Manual. Engineer Manual 1110-2-1100, U.S. Army Corps of Engineers, Washington, D.C. (in 6 volumes).

[5] U.S. Army Corps of Engineers, Hydraulics and Water Quality Section, New England Division, September, 1988. *Tidal Flood Profiles New England Coastline*.

[6] Dean R.R. and Dalrymple, R.A., 1991. *Water Wave Mechanics for Engineers and Scientists*. World Sc. Pub.

[7] Mei, C.C., 1989. *The Applied Dynamics of Ocean Surface Waves*. World Sc. Pub.

[8] Rinne, H. 2009. *The Weibull distribution. A handbook. CRC Press, Chapman and Hall. PP. 784.* Boca Raton, Fl.: CRC Press, Chapman & Hall.

[9] Codiga, D.L. and D.S. Ullman 2010. *Characterizing the physical oceanography of coastal waters off Rhode Island, Part I: Literature review, available observations, and a representative model simulation.* University of Rhode Island. Prepared for the Rhode Island Ocean Special Area Management Plan.

[10] Grilli, S.T., J. Harris, R. Sharma, L. Decker, D. Stuebe, D. Mendelsohn, D. Crowley and S. Decker 2010. *High resolution modeling of meteorological, hydrodynamic, wave and sediment processes in SAMP study are.* University of Rhode Island. Prepared for the Rhode Island Ocean Special Area Management Plan.

Appendix A: Overview of STWAVE equations and implementation

STWAVE is a steady state, finite difference, spectral wave model developed by the US Corps of Engineers [2], based on the conservation of wave action balance equation. STWAVE simulates depth-induced wave refraction and shoaling, current-induced refraction and shoaling, depth- and steepness-induced wave breaking, diffraction, wind-wave growth, and wave-wave interaction and white-capping that redistribute and dissipate energy in a growing wave field. STWAVE is based on the assumption that the relative phases of the spectral components are random, and thus phase information is not tracked (i.e., it is a phase-averaged model). In practical applications, wave phase information throughout a model domain is rarely known accurately enough to initiate a phase-resolving model. Typically, wave phase information is only required to resolve wave-height variations near coastal structures for detailed, near-field reflection and diffraction patterns. Thus, for these situations, a phase-resolving model should be applied.

A.1 STWAVE assumptions

a. *Mild bottom slope and negligible wave reflection.* STWAVE is a half-plane model. Waves reflected from the shoreline thus are neglected. Forward-scattered waves, e.g., waves reflected off a structure but traveling in the +x-direction, are also neglected. The half-plane model also means that wind directions greater than 60° relative to the x-axis will result in under-prediction.

b. *Spatially homogeneous offshore wave conditions.* The input spectrum in STWAVE is constant along the offshore boundary.

c. *Steady-state waves, currents, and winds.* STWAVE is formulated as a steady-state appropriate for wave conditions that vary more slowly than the time it takes for waves to transit the computational grid. Wind waves are in fetch-limited or fully developed conditions.

d. *Linear refraction and shoaling*, *depth-uniform current*, and n*egligible bottom friction.*

A.2 Equations

Interactions of waves with a space-varying current *U(x,y)* are simulated in depth *D(x,y)*, in a reference frame moving with the current. Wave parameters in this frame are denoted with the subscript *r*, for being "relative" to the current, and parameters in the non-moving reference frame have subscript *a*, for "absolute."

The (linear) wave dispersion relationship is given in the moving and absolute reference frames as (Dean and Dalrymple, 1991),

$$\omega_r^2 = gk \tanh kD \quad ; \quad \omega_a = \omega_r + kU \cos(\delta - \alpha) \tag{A.1}$$

with ω and k the wave angular frequency and wavenumber, respectively, δ the local angle of the current and α the local angle of the wave orthogonal direction (i.e., normal to the wave crest) both with respect to the *x*-axis.

Similarly, one defines the local wave celerity C and group velocity C_g in both frames as,

$$C_r = \frac{\omega_r}{k} \quad ; \quad C_a = C_r + U\cos(\delta - \alpha)$$

$$C_{gr} = \frac{C_r}{2}\left(1 + \frac{2kD}{\sinh 2kD}\right) \quad ; \quad C_{ga_i} = C_{gr_i} + U_i \tag{A.2}$$

where subscript $i = 1,2$, denotes both horizontal components in tensor notation.
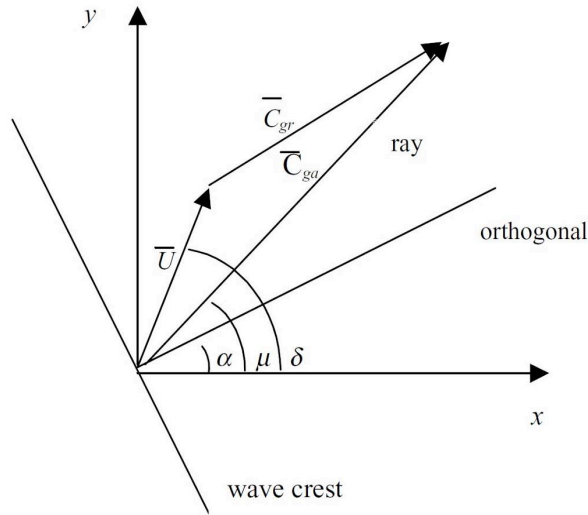
Figure A.1 : Definition sketch of wave and current vectors in STWAVE [2].

The direction vector of the wave orthogonal, also defined as $k_i/k = (\cos\alpha, \sin\alpha)$, is also that of local wave celerity C_a. The direction vector of the wave ray, which indicates the direction of energy propagation, is defined as $(\cos\mu, \sin\mu)$, and is also that of the absolute group velocity C_{ga}. From Eq. (A.2), we thus find,

$$\mu = \arctan\left(\frac{C_{gr}\sin\alpha + U\sin\delta}{C_{gr}\cos\alpha + U\cos\delta}\right)gk\tanh kD \tag{A.3}$$

Note, without current, the wave rays and orthogonals are identical.

In steady-state conditions, the wave orthogonal direction is given by Mei (1989), in a curvilinear coordinate system *(r,n)* as,

$$C_{ga}\frac{d\alpha}{dr} = -\frac{C_r k}{\sinh 2kD}\frac{dD}{dn} - \frac{k_i}{k}\frac{dU_i}{dn} \tag{A.4}$$

where r is coordinate in the direction of the wave ray and n is the coordinate normal to the direction of the wave ray.

The governing equation for steady-state conservation of spectral wave action along a wave ray is given as,

$$C_{ga_i}\frac{\partial}{\partial x_i}\left(\frac{C_a C_{ga}\cos(\mu-\alpha)E(\omega_a,\alpha)}{\omega_r}\right) = \sum\frac{S}{\omega_r} \tag{A.5}$$

where E is wave energy density (divided by $\rho_w g$, with ρ_w the water density) and S is energy source/sink terms (e.g., due to wind energy input and wave breaking dissipation).

Note that no current was used in the simulations in this work, thus all terms in the current frame of reference are equal to those in the absolute frame of reference. However, these equations were presented for completeness as they are used in STWAVE.

A.3 Source/sink terms

Surf-zone wave breaking. The maximum limit on the zero-moment wave height in STWAVE is,

$$H_{m0}^{\max} = 0.1L\tanh kD \tag{A.6}$$

The energy in the spectrum is reduced at each frequency and direction in proportion to the amount of pre-breaking energy in each frequency and direction band. Nonlinear transfers of energy to high frequencies that occur during breaking are not represented in the model. Model grid cells where wave height is limited by Eq. (A.6) are flagged as actively breaking cells.

Wind input. Waves grow through the transfer of momentum from the wind field to the wave field. The flux of energy F_{in}, into the wave field in STWAVE is given by,

$$F_{in} = 0.85\lambda\frac{\rho_a}{\rho_w}C_m\frac{u_*^2}{g} \tag{A.7}$$

where λ is a partitioning coefficient that represents the percentage of total atmosphere to water momentum transfer that goes directly into the wave field (typically 0.75) ρ_a is air density, C_m is mean wave celerity, and $u^* = W(C_D)^{1/2}$ is friction velocity with the wind speed W, and the surface drag coefficient, $C_D = .0012 + .000025W$.

The energy gain to the spectrum is calculated by multiplying the energy flux F_{in} by the equivalent time Δt for the wave to travel across a grid cell of length Δx,

$$\Delta t = \frac{\Delta x}{\beta C_{gm} \cos \alpha_m} \tag{A.8}$$

with β a factor equal to 0.9 for the wind sea portion of the spectrum, and C_{gm} and α_m average group celerity and mean direction relative to the grid of waves in the spectrum. Note, because STWAVE is a half-plane model, only winds blowing toward shore (+x direction) are included.

Wave-wave interaction and white-capping. As energy is fed into the waves from the wind, it is redistributed through nonlinear wave-wave interaction. Energy is transferred from the peak of the spectrum to lower frequencies (decreasing the peak frequency or increasing the peak period) and to high frequencies (where it is dissipated). In STWAVE, the frequency of the spectral peak is allowed to increase with fetch (or equivalently propagation time across a fetch).

Wave energy is dissipated (most notably in an actively growing wave field) through energy transferred to high frequencies and dissipated through wave breaking (white-capping) and turbulent/viscous effects. There is a dynamic balance between energy entering the wave field because of wind input and energy leaving the wave field because of nonlinear fluxes to higher frequencies. These effects are parameterized in STWAVE.

A.4 Numerical implementation

STWAVE is a finite-difference numerical model, formulated on a Cartesian grid with square cells (Fig. A.1). The orientation of the grid is such that the input wave spectrum starts at the offshore boundary, defined by the y-axis, and waves are propagated in the cross-shore (positive x-direction). Wave angles are also defined in a typical Cartesian sense, i.e., measured counterclockwise from the positive x-axis. Wave refraction and shoaling are simulated in STWAVE by applying the conservation of wave action Eq. (A.5), with Eqs. (A.1-4), along backward traced wave rays. Rays are traced in a piecewise manner, from one model grid column to the next. A two-dimensional (i.e, in frequency and direction) wave spectra is set as input along the first grid column (the offshore boundary). For a point on the second grid column, the spectrum is calculated by back tracing a ray for each frequency and direction component of the spectrum. The ray direction, , is determined by Eq. (A.3). Only ray directions propagating toward the shore (-87.5 to +87.5 deg) are included. Energy propagating toward the offshore is neglected.
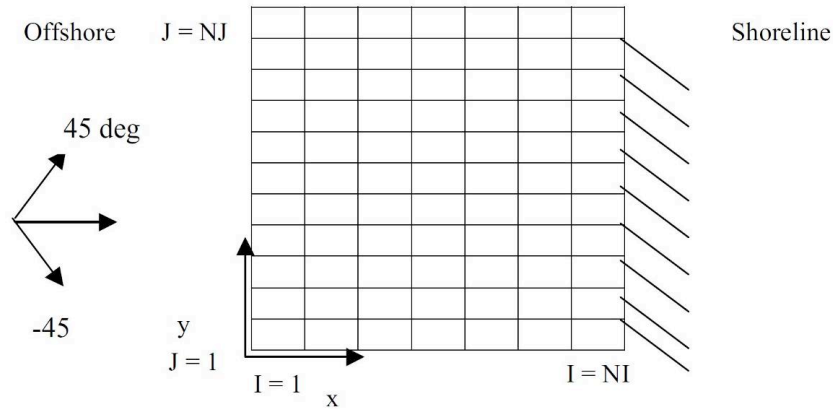
Figure A.2: STWAVE coordinate system and grid definition [2].

More specifically, each wave ray is traced back to the previous grid column, and the length of the ray segment is calculated. Derivatives of depth and current components normal to the wave orthogonal are estimated (based on the orthogonal direction at column at the current column) and substituted into Eq. (A.4), to calculate the wave orthogonal direction at the previous column. Then, the wave number, wave and group celerities, and ray angle in the previous column are calculated. The energy is calculated as a weighted average of energy between the two adjacent grid points in the column and the direction bins. The energy density is corrected by a factor that is the ratio of the 5-degree standard angle bandwidth to the width of the back-traced band to account for the different angle increment in the back-traced ray. The shoaled and refracted wave energy in the current column is then calculated from the conservation of wave action along a ray (A.5).
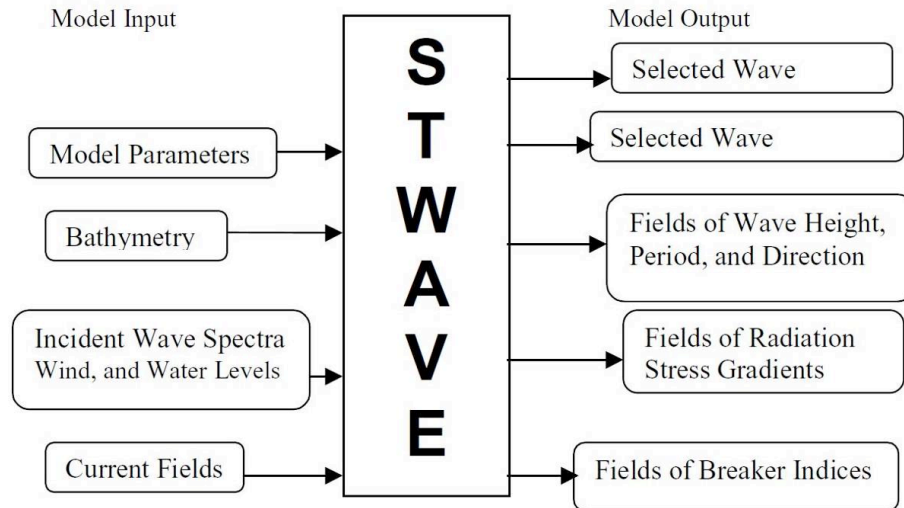

A.5 Input/output files

Figure A.3: STWAVE input and output files [2].

STWAVE takes up to four input files, with the current field being optional (and not used in this study). For brevity, aspects of the input and output files not used in this simulation will not be discussed within this document. Full discussion of input and output files, as well as their contents and examples are available in the software user manual [2].

A.5.1 Model Parameters

The model parameters file contains switches for various options:
- IPRP: Switch for propagation only (1), or propagation and source/sink (0) terms. These terms include wind-wave generation, wave-wave interactions, and whitecapping. These terms were included for simulations in this study.
- IBREAK: Switch for printing (1) or not (0) the field of breaker indices. Breaker indices were printed in this study, as active wave breaking has an effect on wave growth and forcing estimates.

A.5.2 Bathymetry

The bathymetry file determines the simulation domain size and shape, as well as provides the bathymetry for each cell in the domain:
- NI, NJ: The number of cross-shore (x-axis) and long-shore (y-axis) grid cells, respectively.
- DXINC: The grid spacing (meters). This, along with NI and NJ determine the actual spatial size of the simulation domain.
- Depths: The depths are listed starting at (1,NJ) and read in the cross-shore direction. Positive values indicate depth and negative values indicate altitude.

A.5.3 Incident Wave Spectra

The incident wave spectra file contains information on the spectral resolution and extent, as well as various other parameters. Multiple input spectra may be placed in the same file, such that multiple simulations may be run in succession. The parameters W, UDIR, and DADD (discussed below) are uniquely defined for each simulation.
- NF: The number of frequency bins in the spectra. 50 bins was the default value, also used for simulations in this study.
- NA: The number of directional bins in the spectra. This value must be 35, yielding a 5 degree bin width across STWAVE's ±87.5 degrees domain.
- *W*: Wind speed (meters/second), considered constant across the simulation domain.
- UDIR: Wind direction (degrees) relative to the STWAVE coordinate system.
- DADD: Water elevation correction (meters), used for water level changes due to storm surge, tidal changes, etc. This value is also considered constant across the simulation domain.
- Frequencies: A NF-length series of frequencies (Hz). This frequency vector is the same for all simulations in the same file. Accordingly, a standard frequency vector ranging linearly from 0.04 to 0.2 Hz was used in most simulations.
- Spectrum: The energy densities (meters^2/Hz/radian) of the input wave spectrum are listed starting with the lowest frequency and direction and continuing to the

highest direction. This process is then repeated for the second-lowest frequency and so on. The number of points in the spectrum must be NF*NA.

A.5.4 Wave Parameter Fields

The wave parameters (significant wave height H_{m0}, peak period T_p, and mean direction α) are printed for each grid cell in the simulation. The values are written in the same order as the bathymetry values, starting at (1,NJ) and proceeding in the cross-shore direction to (NI,NJ), then moving over one row to begin again at (1,NJ-1). This process is performed for wave height, then period, then direction.

A.5.5 Breaker Index Field

The breaker indices are printed as binary indices, with 1 signaling breaking and 0, no breaking. The values are written in the same order as the wave parameter fields and bathymetries.